Applied Energy 278 (2020) 115581

Contents lists available at ScienceDirect

Applied Energy

journal homepage: www.elsevier.com/locate/apenergy

Management of an island and grid-connected microgrid using hybrid economic model predictive control with weather data

Danilo P. e Silva [a,1], José L. Félix Salles [b,*], Jussara F. Fardin [b], Maxsuel M. Rocha Pereira [c]

[a] Federal Institute of Education, Science and Technology of Espírito Santo, Serra, E.S., Brazil
[b] Electrical Eng. Department, Federal University of Espírito Santo, Vitória, E.S., Brazil
[c] Industrial Technology Department, Federal University of Espírito Santo, Vitória, E.S., Brazil

GRAPHICAL ABSTRACT

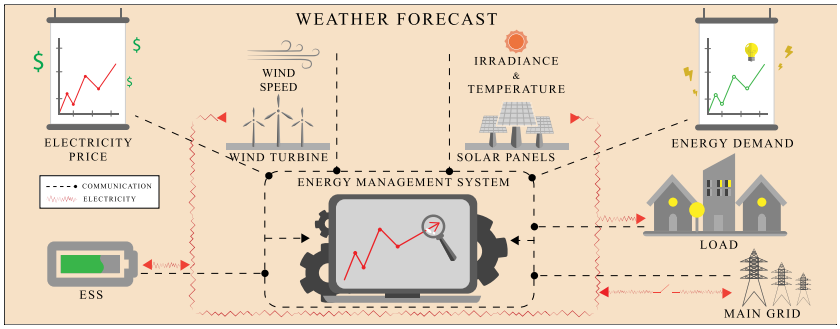

ARTICLE INFO

Keywords:
Microgrid
Renewable energy resources
Optimization
Hybrid economic model predictive control
Energy management system
Weather data

ABSTRACT

Microgrid management is a multi-objective problem that involves purchasing and selling energy, time-variant renewable generation, and maintenance costs. The microgrid can operate autonomously on an island or through mode connected with the main grid. This paper proposes an original optimization model for the management of an isolated microgrid that allows the automatic grid connection to provide ancillary services to the main grid, such as selling the excess renewable generation and purchasing electricity to charge the battery bank. The proposed optimization is formulated via hybrid economic model predictive control using weather forecasts performed by a mesoscale meteorological model. It includes new constraints to meet a specific connection/disconnection regulation, such as the minimum connection/disconnection time and the maximum connection frequency. This paper also proposes a new hybrid model of a battery bank that includes the grid connection/ disconnection. Furthermore, the hybrid models of renewable energy sources convert weather data to the wind and photovoltaic power by using the mixed logical dynamical framework. The proposed algorithm is sensitive to the forecasting error, which causes variations of 1% in the met demand, 27.3% in the battery bank costs, and 13.3% in the financial profits. Compared to multi-period mixed integer linear programming and rule-based strategy, we show that the proposed controller manages the microgrid more safely (i.e., it provides state of charge below its critical value during a period less than 25% of that offered by other strategies). In locations with high energy generation, only the proposed optimization furnishes energy sale profit.

* Corresponding author.
E-mail address: jleandro@ele.ufes.br (J.L.F. Salles).
[1] Ph.D. student in electrical engineering at Federal University of Espírito Santo.

https://doi.org/10.1016/j.apenergy.2020.115581
Received 9 January 2020; Received in revised form 4 July 2020; Accepted 20 July 2020
Available online 5 August 2020

1. Introduction

Technologies based on renewable energy sources (RES) such as wind turbines, photovoltaic panels (PV), and fuel cells have become essential for meeting the growing demand for sustainable energy and the world's economic development. Renewable energies accounted for the highest share in primary energy production in the European Union in 2018 (28.4%) [1]. From the total renewable energy produced, 57% corresponded to photovoltaic and wind power generation. In 2019, the United States produced 4.18 trillion kilowatt hours of electricity, and the RES generation corresponded to 19% of the total energy produced [2]. The RES generation in China increased 6% in 2019 when compared to 2018 [3]. In Brazil, 9.9% of electricity generation-installed capacity (162.8 GW) in 2018 corresponds to the wind and photovoltaic generation [4]. This growth in renewable energy use around the world has increased the uncertainties concerning the electric power systems due to the intermittent renewable power generation. In this scenario, a microgrid (MG) is a promising approach [5,6] because of its ability to operate with bidirectional power flow as well as independently or connected to the main grid. A typical MG is composed of electric charges, an energy storage system (ESS), RES, and fossil fuel power generation.

The complete formulation of the optimal operation problem of MG requires mathematical models related to the energy storage system, power exchange with the main grid, data forecasting, and demand-side management policies [7]. Several mathematical models developed for MG have been presented in the literature for real-time operation, demand-side management [8], and optimization. The authors in [9] formulate a stochastic correlation model between generation and demand of different MGs, and the work [10] proposed a support decision-making framework for investments in distributed generation of three different MGs. The authors in [10] use the mixed integer programming (MILP) formulation to determine the minimal cost capacity and operation of the distributed energy resources in a microgrid. The work [11] proposed a real-time simulator for MG monitoring, and the paper [12] considered smart electrical loads in the MG mathematical formulation. Finally, the authors [13–15] used the mixed logic dynamic (MLD) [16] framework for MG modeling.

The economic dispatch problem for MG aims to perform fast operational decisions along a planning horizon of a few minutes to 1 h ahead to minimize energy and operational and maintenance (O&M) costs and maximize energy sales to the main grid [5]. The decisions taken in this optimization problem are the amount of power that each RES should provide to meet the loads, the amount of energy that should be purchased or sold to the main grid, and when the MG should disconnect from the main grid. Several optimization techniques have been proposed in order to solve the economic dispatch problem for MG in the last 5 years, including the following: genetic algorithm [17,18], evolutionary algorithms [19], exchange market algorithm [20], differential evolution algorithm [21] and particle swarm optimization algorithms [22,23], mixed-integer programming [24–26], rolling horizon, [27–29], and model-based predictive control (MPC) [30].

Other works on the economic dispatch problem analyzed MGs operating on grid-connected and grid-disconnected modes. However, they did not consider the autonomy of the management system to decide when to switch between these two operational modes. The paper [31] used the multi-objective genetic algorithm for the optimal management of a battery system with photovoltaic panels under programmed grid-disconnection when predictable blackouts occur in the main grid. However, it would be ideal if an MG had the autonomy to detect the main grid failures before the blackout occurrence and carried out the disconnections automatically. In [32], the authors presented the affine arithmetic MPC-based approach of combined heat and power microgrid that considers both connected and isolated operation modes. The MG operational performance is analyzed separately in these two scenarios (disconnected or connected modes). However, the automatic grid connection/disconnection of MG was not taken into account. In locations where the consumer unit has a high probability of main grid interruptions due to poor quality of service [33], it is convenient and viable that an MG stay in isolated mode. Moreover, it must have the autonomy of eventually connecting to the grid and offering ancillary services such as voltage regulation, reduction of peak demand, and harmonic filtering. During the grid connection, the MG can sell the excess renewable energy generation to the main grid to avoid energy waste in the dump load [34] when the battery is charged.

The weather data forecasting is important information for microgrid management because it determines the power generated from RES [29] and the thermal and electrical loads that can be fed by the microgrid [35–37]. The association of feedback control strategies and forecasting techniques in the decision variables of the economic dispatch problem are reasons for the success of MPC in microgrid management. However, some studies that used MPC [13] ignored weather data, and the solutions obtained reflect ideal representations of the MG operating conditions. They did not address possible contingencies derived from the operation under real scenarios of meteorological events. Some articles that used MPC commented on the need to perform forecasts, but left in the background the information about the weather forecasting techniques and the impact of the forecasting errors on the results obtained [15,35,37]. Instead of using meteorological data, other works preferred to deal only with historical power data to obtain renewable energy generation [30,32,38–41].

It is challenging to forecast renewable power using only historical power data because of the shading effect on the photovoltaic panels. However, we can achieve better power forecasting results by performing irradiance forecasts through techniques that detect sunny days, cloudy days, and rainy days [42]. Another challenging issue is the effect of the wind power saturation when the wind speed frequently leaves the range between the cut-in and cut-off speed values (minimum and maximum), inflicting a strong nonlinearity on the wind power time series. Therefore, power forecasting models require nonlinear forecasting techniques, such as those based on the support vector machine [43]. Thus, nonlinear models have their own characteristics that depend on a specific renewable energy generator already installed in an MG.

Conversely, the use of weather data to forecast renewable energy generation and electrical and thermal demands can detect weather disturbances such as sudden changes in temperature, irradiance, and humidity, which can affect microgrid management. Moreover, it is possible to use mesoscale meteorological models, such as the weather research and forecasting (WRF) model [44], for the generation of dynamic and thermodynamic data from the atmosphere. The advantage of this forecasting method is that it does not depend on the implementation of the physical installation of surface meteorological stations. In this case, the WRF model allows us to carry out feasibility studies of the technique applied in any location, based on the geographic coordinates of the current place, or the future installation of an MG. However, the simple application and indiscriminate use of numerical models can produce results far from the reality if the calibration of the WRF model and the representation of the physical processes operating in the region are not correct. To avoid these deficiencies, the WRF model must be adjusted correctly. For this, current research exists on the gathering of knowledge and critical analysis of the simulations obtained by this forecasting model. However, the use of meteorological data using mesoscale models is subject to significant errors compared to the power forecast using models based on historical power data.

Considering the literature studied, we observed few articles that apply MPC in MG management and perform forecasts of weather data to obtain renewable energy generation. The article [14] manages an MG connected to the main grid through the hybrid MPC (HMPC) controller. These authors used neural networks in conjunction with autoregressive integrated moving average models to perform forecasts on irradiance, temperature, wind speed, humidity, and wind direction. Although this article presents the MLD model of the energy storage

system in detail, it does not describe the solar and wind energy models for converting weather data into power. Moreover, the HMPC cannot perform the connection /disconnection of MG with the main grid. In [29], the authors considered the uncertainty in the wind speed forecast using the max–min method [42] and formulated the MILP optimization problem combined with the rolling horizon and stochastic programming. However, these authors modeled only wind generation using weather data and considered an MG always connected to the main grid. The paper [35] presented the temperature control of a room through HMPC using data of irradiance and external temperature in the MG installation locality. These authors used stochastic programming to model the irradiance forecast to obtain solar power. However, they presented only the solar power model using irradiance data and did not formulate the HMPC to manage the connection and disconnection of an MG with the main grid. In [45], the authors used the stochastic MILP optimization and the rolling horizon algorithm to manage an isolated MG. They performed wind speed and irradiance forecasts from the WRF system combined with statistical methods, using the persistent techniques and clear-sky index for irradiance [46]. Besides, they also determined the solar and wind power forecasting models of solar and wind power but did not manage the connection/disconnection of an MG with the main grid.

This paper aims to fill the gap in the literature concerning the MG management using MPC with weather data forecasted by the WRF model, considering the grid connection and disconnection. We propose the MG economical dispatch algorithm through the hybrid economic model predictive control (HEMPC) approach that uses weather data. The optimization model allows an MG to operate in the island mode and eventually in the grid-connected mode to offer energy sale services to the main grid when there is a surplus of renewable energy. The proposed optimization algorithm includes constraints on meeting a specific MG connection and disconnection regulation, such as the minimum connection/disconnection time and the maximum connection frequency. This paper also proposes a new hybrid model of a battery bank that takes into account the connection and disconnection of an MG with the main grid. In grid-connection mode, the main grid charges the battery bank, viewing it as a load. Finally, the hybrid ESS model proposed here has improvements in the switching logic and the continuous dynamics compared to the model proposed in [47].

Another original contribution is the PV panel hybrid modeling based on the equivalent circuit equation [48]. Some PV panel models found in the literature calculate the power through theoretical equations based on the PV panel area [49], irradiance, temperature, wind speed, latitude, and longitude [50]. However, these works do not consider PV power saturation. The advantage of hybrid models over theoretical power-supply equations is that they can convert some types of nonlinearities into logical propositions, which may include constraints and continuous and binary variables. The paper in [51] proposed a wind turbine MLD model, and it used the HMPC strategy to improve the wind turbine performance. However, these authors did not present the wind turbine modeling in detail, as we have presented here. Other hybrid models proposed in this paper, such as electrical loads and purchasing and selling electrical energy, were based on previous works [13,15,41]. However, these articles lacked details about the discrete hybrid automata (DHA) approach [52]. DHA is a dynamic system that describes the temporal evolution of the set of logic (or discrete) and real (or continuous) variables.

The main original contributions of this article can be summarized as follows:

1. The objective function considers the connected and isolated modes of the MG operation with the main grid to provide ancillary services, to purchase or sell energy, and to avoid energy waste in the dump load.
2. The minimum time interval for MG to stay grid connected and the maximum number of grid connections over a time interval.
3. The photovoltaic hybrid model uses the MLD structure with weather data such as irradiance and temperature.
4. The photovoltaic and wind power forecasts obtained from the global WRF forecasting model of meteorological data.
5. The detailed modeling of the wind turbine obtained through the discrete hybrid automata approach.

The proposed management algorithm assumes that the MG has decision-making autonomy to perform connections to the main grid, offering and receiving services from the utility, such as battery bank charging. Besides, it belongs to the secondary control level of hierarchical control structure presented in [53]. This control level is responsible for the reliability, safety, and economic operation of MGs in both connected and isolated modes through the energy management system (EMS). The EMS is a centralized control structure that optimizes an MG's economic dispatch according to ESS information, RES forecast, electric power loads, and electricity prices [54].

The remainder of this article is organized as follows: Section 2 presents the hybrid modeling of PV, wind turbine, and battery bank by considering weather data. Section 3 formulates the cost function and constraints of the optimization problem to include the connection and disconnection operations of an MG with the main grid. We also present in Section 3 the HEMPC algorithm. Section 4 shows the study of cases from computational simulations using real weather data from different meteorological characteristics. It analyzes the computational performance and forecasting error sensibility of the algorithm. Moreover, it compares the proposed algorithm with the rule-based strategy and the MILP multi-period optimization. Finally, we conclude this paper in Section 5.

2. Microgrid modeling

In this section, we present each MG equipment model through DHA. DHA is composed of four components: switch affine system (SAS), event generator (EG), finite state machine (FSM), and mode selector (MS). The EG extracts and generates logical signals from the SAS. These external logics enable the transition of FSM states. A MS processes all logic signals in order to choose new continuous SAS dynamics. The parameters of proposed DHA models depend on the weather data measured at each time kT_s, where T_s is the sample time. For notation simplification, we omitted T_s in all equations presented here. The proposed MG model makes the following assumptions:

1. The existence of the following MG equipment: solar panels, wind turbine, ESS having a battery bank, electric charges, and weather data acquisition through a local meteorological station.
2. The secondary level of the hierarchical control structure is not affected by the transient behaviors of the primary level dynamics.
3. The connection and disconnection duration times of an MG to the main grid are a few seconds, and they do not interfere in the second control system level, which is updated in minutes.
4. The connection and disconnection operations of an MG to the main grid do not affect its stability.
5. All MG disconnections from the main grid are intentional (i.e., there are not disconnections due to failures).
6. The pitch and frequency control of the wind generator track its maximum power.
7. The charging and discharging efficiencies of the battery bank are assumed constant.

2.1. Photovoltaic generation

The equivalent circuit of the photovoltaic array [48] is represented by

$$I(k) = I_{sc} \cdot \lambda(k) - \frac{I_{sc}}{e^{\frac{qA}{n k_B T(k)}}} \cdot \left[e^{\frac{qA}{n k_B T(k)}} \cdot e^{\frac{V(k)}{V_{oc}}} - 1\right] \quad (1)$$

This equation depends on the irradiance variation $\lambda(k)$, the ambient temperature $T(k)$, the open-circuit voltage V_{oc}, the short circuit current I_{sc}, the ideality factor A, Boltzmann constant k_B, the elementary charge of the electron q, and the number of cells of the photovoltaic module n. We used the maximum power point tracking algorithm (MPPT) to calculate the maximum power ($P_{MPPT}(k)$) at each instant $k = 0, 1, 2, \ldots$ according to the following steps:

1. Read the measured irradiance and temperature ($\lambda(k), T(k)$) at the current instant k.
2. Vary the PV voltage at instant k ($V(k)$) from 0 to V_{oc} and calculate from Eq. (1) the power curve versus voltage through the relation $P_{pv}(k) = V(k)I(k)$.
3. Interpolate the power curve versus PV voltage through a polynomial of order n, shown in (2), that relates the power generated in the panel ($P_{pv}(k)$) with the applied PV voltage.
4. Calculate from Eq. (2) the maximum power at instant k ($P_{MPPT}(k)$).

$$P_{pv}(k) = d_n(k)V^n(k) + d_{n\text{-}1}(k)V^{n-1}(k) + \cdots + d_1(k)V(k) + d_0(k) \tag{2}$$

where $d_0, d_1, \ldots, d_n$ are parameters that depend on irradiance and temperature.

The photovoltaic panel DHA model is represented by the logical sentences (3), (4), and (5). The selector mode, given by (3), selects SAS dynamics defined by (4) according to the event generator binary variable $\delta_{pv1}(k)$ given by (5). If the calculated power ($P_{pv}(k)$) is greater than the PV nominal power ($\delta_{pv1}(k) = 1$) for a given irradiance and temperature, then the power saturates at value P_{pvsat}. The switching affine system represented by (4) changes the maximum generation power between the dynamics described in (2) and the saturation of the nominal power, according to the mode selector.

$$MS: m_{pv}(k) = \begin{cases} 1 & \text{if } \neg\delta_{pv1}(k) \\ 2 & \text{if } \delta_{pv1}(k) \end{cases} \tag{3}$$

$$SAS: \begin{cases} x_{pv}(k+1) = P_{pv}(k) & \text{if } m_{pv}(k) = 1 \\ x_{pv}(k+1) = P_{pvsat} & \text{if } m_{pv}(k) = 2 \end{cases} \tag{4}$$

$$EG: \{[\delta_{pv1}(k) = 1] \leftrightarrow [P_{pv}(k) \geq P_{pvsat}] \tag{5}$$

2.2. Wind generation

The energy conversion system of a wind turbine is characterized by a power curve provided by the manufacturer that relates the wind power ($P_w(k)$) and the wind speed ($v(k)$) on the turbine. On a pitch-controlled wind turbine, the ratio between wind power $P_w(k)$ and its nominal power P_{wn} has four logic states defined by four operational regions (see Fig. 1):

- No generation (idle state) for speeds lower than v_{cutin}.
- Maximum power point tracking (MPPT) state for speeds ranging from v_{cutin} to nominal speed v_n.
- Nominal state where the wind turbine reaches its rated power for speeds greater than v_n.
- Cut-off state when the wind speed exceeds v_{cutoff} and the turbine stops, or it operates at shallow speed with generate power equal to P_{cutoff}.

Through the points extracted in the MPPT region of Fig. 1, we determined the wind power from a polynomial interpolation given by

$$P_w(k) = a_n v^n(k) + a_{n\text{-}1}v^{n-1}(k) + \cdots + a_1 v(k) + a_0 \tag{6}$$

where $a_0 \ldots a_n$ are polynomial constants. The wind power provided by the polynomial (6) is closer to the manufacturer's data than the one provided by [51], which linearized the maximum power point tracking region in four operational points.

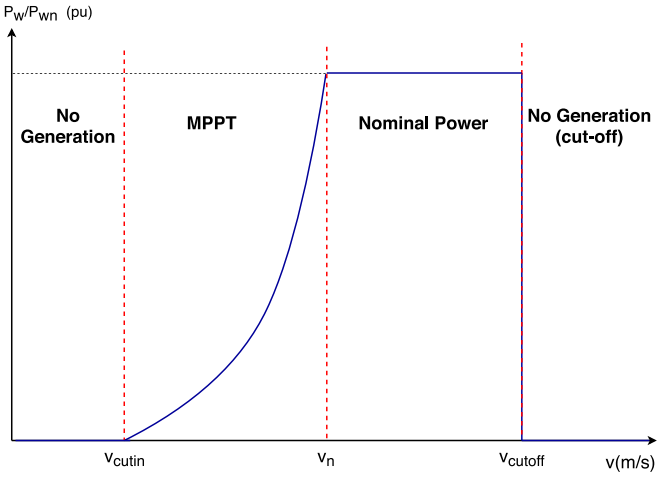

Fig. 1. The pitch-controlled wind turbine curve.

The proposed wind generation DHA model has the finite state machine (FSM) defined by (7). This FSM evolves through discrete events between operational states: idle (x_{wb1}), MPPT (x_{wb2}), nominal (x_{wb3}), and cut-off (x_{wb4}). The event generator shown in (8) and the binary variable op indicate that the wind generator is operating below its rated power, and pn indicates that the generator is operating at its rated power. Each state generated by FSM can be accessed by all other states, depending on the transition event.

The selection rules between the dynamics in (10) are defined by the mode selector in (9). For example, if the wind turbine is in an idle state (x_{wb1}), then $m_w(k) = 1$ and consequently $x_w(k+1) = 0$ in SAS. If only event δ_{w1} is disabled ($v(k) \geq v_{cutin}$), the turbine FSM changes from the idle state (x_{wb1}) to the MPPT state (x_{wb2}) and the MS makes $m_w(k) = 2$ and selects $x_w(k+1) = P_w(k)$ on SAS.

$$FSM: x_{wb} = \begin{cases} x_{wb1} & \text{if } (x_{wb1} \wedge \delta_{w1}) \vee (x_{wb2} \wedge \delta_{w1}) \\ & \vee (x_{wb3} \wedge \delta_{w1}) \vee (x_{wb4} \wedge \delta_{w1}) \\ x_{wb2} & \text{if } (x_{wb1} \wedge op) \vee (x_{wb2} \wedge op) \\ & \vee (x_{wb3} \wedge op) \vee (x_{wb4} \wedge op) \\ x_{wb3} & \text{if } (x_{wb1} \wedge pn) \vee (x_{wb2} \wedge pn) \\ & \vee (x_{wb3} \wedge pn) \vee (x_{wb4} \wedge pn) \\ x_{wb4} & \text{if } (x_{wb1} \wedge \delta_{w3}) \vee (x_{wb2} \wedge \delta_{w3}) \\ & \vee (x_{wb3} \wedge \delta_{w3}) \vee (x_{wb4} \wedge \delta_{w3}) \end{cases} \tag{7}$$

$$EG: \begin{cases} [\delta_{w1} = 1] \leftrightarrow [v \leq v_{cutin}] \\ [\delta_{w2} = 1] \leftrightarrow [v \geq v_n] \\ [\delta_{w3} = 1] \leftrightarrow [v \geq v_{cutoff}] \\ [op = \neg\delta_{w1} \wedge \neg\delta_{w2}] \leftrightarrow [v > v_{cutin} \wedge v < v_n] \\ [pn = \delta_{w2} \wedge \neg\delta_{w3}] \leftrightarrow [v \geq v_n \wedge v < v_{cutoff}] \end{cases} \tag{8}$$

$$MS: m_w(k) = \begin{cases} 1 & \text{if } x_{wb1}(k) \\ 2 & \text{if } x_{wb2}(k) \\ 3 & \text{if } x_{wb3}(k) \\ 4 & \text{if } x_{wb4}(k) \end{cases} \tag{9}$$

$$SAS: \begin{cases} x_w(k+1) = 0 & \text{if } m_w(k) = 1 \\ x_w(k+1) = P_w(k) & \text{if } m_w(k) = 2 \\ x_w(k+1) = P_{wn} & \text{if } m_w(k) = 3 \\ x_w(k+1) = P_{cutoff} & \text{if } m_w(k) = 4 \end{cases} \quad (10)$$

2.3. ESS - Battery bank

The DHA model of battery bank represents different dynamics according to the MG operational modes: isolated or connected to the main grid. In the logical equations presented in (11), when the state of charge (SOC) $S(k)$ reaches its maximum value, the battery bank will be charged and $\delta_{s1}(k) = 1$. Otherwise, the batteries have not reached their maximum SOC. The event $\delta_{s2}(k) = 1$ occurs when the MG is connected to the main grid, and the battery bank is not charged. The mode selector defined by (12) chooses the SAS dynamics represented by (13) according to the variable $u_g(k)$ defined in (14).

$$EG: \begin{cases} [\delta_{s1}(k) = 1] \leftrightarrow [S(k) \geq S_{max}] \\ [\delta_{s2}(k) = 1] \leftrightarrow [u_g(k) \vee \neg\delta_{s1}(k)] \end{cases} \quad (11)$$

$$MS: m_s(k) = \begin{cases} 1 & \text{if } \neg u_g(k) \\ 2 & \text{if } u_g(k) \end{cases} \quad (12)$$

$$SAS: \begin{cases} S(k+1) = S(k) - \frac{\eta T_s}{C_{max}} \cdot i_1(k) - x_b^s & \text{if } m_s(k) = 1 \\ S(k+1) = S(k) + \frac{\eta T_s}{C_{max}} \cdot i_2(k) - x_b^s & \text{if } m_s(k) = 2 \end{cases} \quad (13)$$

$$u_g(k) = \begin{cases} 1 & \text{if MG is grid-connected} \\ 0 & \text{if MG is isolated} \end{cases} \quad (14)$$

In the logical equation system (13), x_b^s represents the self-discharge current of battery bank, $i_1(k)$ refers to the charge/discharge current when the MG is isolated, $i_2(k)$ is the charge current of the battery bank when the MG is grid-connected. $i_1(k)$ is determined from Eq. (15a) (i.e., it is equal the load current $i_L(k)$ minus the PV $i_{pv}(k)$ and wind generator $i_w(k)$ currents). The battery bank is charged when $i_1(k)$ is negative; otherwise, the battery bank is discharged. $i_2(k)$ is the charger current supplied to the battery bank when the MG is connected. If $\delta_{s2}(k) = 1$ in (11), then the battery bank is charged. In this case, the charger stops supplying power to the battery bank (i.e., $i_2(k) = 0$).

$$i_1(k) = i_L(k) - i_{pv}(k) - i_w(k) \text{ if } \neg u_g(k) \quad (15a)$$

$$i_2(k) = i_{ch}(k)\delta_{s2}(k) \text{ if } u_g(k) \quad (15b)$$

Therefore, when the MG is connected to the grid, the battery bank charger is a load for the main grid, which the demand is given by

$$D_{ch}(k) = \delta_{s2}(k) \cdot D_{c2}(k) \quad (16)$$

where $D_{c2}(k) = i_{ch}(k) \times V_b$ and V_b is the battery bank voltage.

2.4. Electrical loads

We consider that there is a total of n_c controllable electrical loads through contactors. Each contactor is represented by a binary variable $c_h, h = 1, \ldots, n_c$. Each load L_h has a power demand D_h. The controllable loads DHA can be represented by the expressions in (17), (18), and (19):

$$EG: \begin{cases} [c_1(k) = 1] \leftrightarrow [L_1 = D_1] \\ [c_2(k) = 1] \leftrightarrow [L_2 = D_2] \\ \quad \vdots \\ [c_{n_c}(k) = 1] \leftrightarrow [L_{n_c} = D_{n_c}] \end{cases} \quad (17)$$

$$MS: m_l(k) = \begin{cases} 1 & \text{if } g_{l1}(c_1, c_2, \ldots, c_n) = 0 \cdots 01 \\ 2 & \text{if } g_{l2}(c_1, c_2, \ldots, c_n) = 0 \cdots 10 \\ 3 & \text{if } g_{l3}(c_1, c_2, \ldots, c_n) = 0 \cdots 11 \\ \vdots & \\ \varrho & \text{if } g_{l\varrho}(c_1, c_2, \ldots, c_n) = 1 \cdots 11 \end{cases} \quad (18)$$

$$SAS: D_c(k) = \begin{cases} 0 & \text{if } m_l(k) = 1 \\ D_2 & \text{if } m_l(k) = 2 \\ \vdots & \\ D_\varrho & \text{if } m_l(k) = \varrho \end{cases} \quad (19)$$

where $\varrho = 2^{n_c}$ e $g_l(.)$ is a function that represents a binary number with n_c bits such that $g_l(c_1, c_2, \ldots, c_{n_c}) = c_{n_c} \cdots c_2 c_1$. The total controlled demand is the sum of all turned on loads, which is represented by

$$D_c(k) = \sum_{h=1}^{n_c} c_h(k) D_h(k) \quad (20)$$

For example, if we have two controllable loads with demands D_1 and D_2, the SAS in (19) will have four dynamics and the possible values of loads are $D_c = \{0, D_1, D_2, D_1 + D_2\}$. Usually, an MG also has critical loads (i.e., loads that are non-controllable and always remain turned on). The total demand of the electric load, including the critical loads, are defined by

$$D_L(k) = \sum_{h=1}^{n_c} c_h(k) D_h(k) + \sum_{i=1}^{n_l} D_i(k) \quad (21)$$

where n_l is the number of critical loads and D_i is the ith critical load.

2.5. Electricity price

An MG can purchase or sell electrical power at prices $c_p(k)$ and $c_s(k)$ respectively, when it is connected to the grid. The DHA model of electricity price used in this paper was proposed in [13]. The expressions (22), (23), and (24) describe this model:

$$EG: \{[\delta_g(k) = 1] \leftrightarrow [P_g(k) \geq 0] \quad (22)$$

$$MS: m_p(k) = \begin{cases} 1 & \text{if } \neg\delta_g(k) \\ 2 & \text{if } \delta_g(k) \end{cases} \quad (23)$$

$$SAS: C_g(k) = \begin{cases} c_s(k) P_g(k) & \text{if } m_p(k) = 1 \\ c_p(k) P_g(k) & \text{if } m_p(k) = 2 \end{cases} \quad (24)$$

where $C_g(k)$ is the cost of energy and $P_g(k)$ is the instantaneous power balance of the connected MG, defined in (25).

2.6. Power balance

The power balance defined in (25) represents the difference between consumption and generation of energy, (i.e., it is the sum of all load demands of the MG, including the battery bank charger, minus the sum of PV and wind power generations).

$$\begin{aligned} P_g(k) &= D_L(k) + D_{ch}(k) - P_w(k) - P_{pv}(k) \\ &= \sum_{i=1}^{n_l} D_i(k) + \sum_{h=1}^{n_c} c_h(k) D_h + \delta_{s2}(k) D_{c2}(k) - P_w(k) - P_{pv}(k) \end{aligned} \quad (25)$$

The second equality in the above expression separates the controllable loads from the critical loads. The power balance depends on the operational policy of the MG, as explained as follow:

- If the power balance $P_g(k)$ has a negative sign, then generation is larger than consumption; otherwise, consumption is larger than generation.

- If the MG is isolated, $P_g(k)$ is the charge or discharge power of the battery bank.
- If the MG is connected to the grid, $P_g(k)$ is the power exchanged with the main grid.

2.7. Connection and disconnection conditions

We assumed that the power utility allows the connection and disconnection of the MG to the main grid during the minimum time intervals τ_c and τ_i, respectively. The following expressions determine these time intervals:

$$\tau_c = \min(T_{up}, N)T_s \tag{26}$$

$$\tau_i = \min(T_{down}, N)T_s \tag{27}$$

where T_{up} and T_{down} are the minimum numbers of samples required for the MG to remain grid connected and isolated, respectively; T_s is the sample time; and N is the forecasting horizon.

Let us denote by $\xi_{hon}(k)$ and $\xi_{hoff}(k)$ the variables that count the number of samples remaining that are necessary to enable the connection or disconnection of an MG from the current sample. The last connection and disconnection of an MG occurs at samples k_c and k_i, respectively. These counters satisfy the following equations:

$$\xi_{hon}(k+1) = \xi_{hon}(k) - 1, \text{ for } k \geq k_c \text{ and } \xi_{hon}(k_c) = \frac{\tau_c}{T_s} \tag{28}$$

$$\xi_{hoff}(k+1) = \xi_{hoff}(k) - 1, \text{ for } k \geq k_i \text{ and } \xi_{hon}(k_i) = \frac{\tau_i}{T_s} \tag{29}$$

To guarantee positive values for these counters, we defined the binary variables $\delta_{hon}(k)$ and $\delta_{hoff}(k)$ by the following expressions:

$$EG: \begin{cases} [\delta_{hon}(k) = 1] \leftrightarrow [\xi_{hon}(k) \geq 0] \\ [\delta_{hoff}(k) = 1] \leftrightarrow [\xi_{hoff}(k) \geq 0] \end{cases} \tag{30}$$

Let us define the binary states $holdon(k)$ and $holdoff(k)$ that indicate which counter $\xi_{hon}(k)$ and $\xi_{hoff}(k)$ are enabled, respectively. These states satisfy the FSM (31), which detects the MG connection and disconnection times and checks whether $\delta_{hon}(k)$ and $\delta_{hoff}(k)$ are enabled.

$$FSM: \begin{cases} holdon(k+1) &= ((u_g(k) \wedge \neg u_g(k-1)) \vee holdon(k)) \wedge \delta_{hon}(k) \\ holdoff(k+1) &= ((\neg u_g(k) \wedge u_g(k-1)) \vee holdoff(k)) \wedge \delta_{hoff}(k) \end{cases} \tag{31}$$

When the binary states $holdon(k)$ and $holdoff(k)$ are disabled, the counters $\xi_{hon}(k)$ and $\xi_{hoff}(k)$ are reset through the MS in (32) and the SAS in (33).

$$MS: m_{clk}(k) = \begin{cases} 1 & \text{if } holdon(k) \\ 2 & \text{if } \neg holdon(k) \\ 3 & \text{if } holdoff(k) \\ 4 & \text{if } \neg holdoff(k) \end{cases} \tag{32}$$

$$SAS: \begin{cases} \xi_{hon}(k+1) = \xi_{hon}(k) - 1 & \text{if } m_{clk}(k) = 1 \\ \xi_{hon}(k+1) = min(T_{up}, N) & \text{if } m_{clk}(k) = 2 \\ \xi_{hoff}(k+1) = \xi_{hoff}(k) - 1 & \text{if } m_{clk}(k) = 3 \\ \xi_{hoff}(k+1) = min(T_{down}, N) & \text{if } m_{clk}(k) = 4 \end{cases} \tag{33}$$

For example, if the MG is connected to the main grid ($u_g(k) = 1$), the $holdon(k)$ state is enabled and the variable $m_{clk}(k) = 1$ selects the SAS dynamic that decrements $\xi_{hon}(k)$. When $\xi_{hon}(k)$ is less than zero, the $holdon(k)$ state becomes inactive and the counter changes its SAS dynamics according to the mode selector $m_{clk}(k) = 2$. In this situation, the MG has reached its minimum connection time and can remain connected or not.

The MG cannot be disconnected from the grid while the binary state $holdon(k)$ is enabled (i.e., while $\xi_{hon}(k)$ is counting); thus, we have

$$u_g(k) = 1 \text{ if } holdon(k) = 1 \tag{34}$$

and analogously, the Boolean relation in (35) describes that an MG cannot be connected to the grid while $\xi_{hoff}(k)$ is enabled.

$$u_g(k) = 0 \text{ if } holdoff(k) = 1 \tag{35}$$

We also assumed that the power utility has a maximum number (nc_{max}) of MG connections with the main grid during any time interval $[iT_c, (i+1)T_c]$, $i = 0, 1, 2$, where T_c is a time period specified by the power distribution company. These intervals have the sampling period T_s, so the maximum number of samples in each of these intervals is $ns_{max} = T_c/T_s$. The time interval from iT_c to $kT_s \in [iT_c, (i+1)T_c]$ is indicated by the real variable $\xi_s(k) \in [0, T_c]$. Let $\delta_{\xi}(k)$ be the binary variable, which always resets $\xi_s(k)$ according to the following logical and dynamical system:

$$SAS: \begin{cases} \xi_s(k+1) = \xi_s(k) + T_s & \text{if } m_c(k) = 1 \\ \xi_s(k+1) = 0 & \text{if } m_c(k) = 2 \end{cases} \tag{36}$$

$$MS: m_c(k) = \begin{cases} 1 & \text{if } \neg\delta_{\xi} \\ 2 & \text{if } \delta_{\xi} \end{cases} \tag{37}$$

Let us denote by $\xi_c(k)$ the number of MG connections to the main grid from instant $t = iT_c$ to instant $t = kT_s \in [iT_c, (i+1)T_c]$. The transition from the isolated mode to the connected mode at time $t = kT_s$ is detected by the binary variable $\delta_c(k)$ and the maximum number of connections within each time interval $[iT_c, (i+1)T_c]$ is indicated by the binary variable $\delta_{cmax}(k)$. From these definitions we determined the logical and dynamical system:

$$EG: \begin{cases} [\delta_c(k) = 1] \leftrightarrow [u_g(k) \wedge \neg u_g(k-1)] \\ [\delta_{cmax}(k) = 1] \leftrightarrow [\xi_c(k) > nc_{max}] \\ [\delta_{\xi}(k) = 1] \leftrightarrow [\xi_s(k) > T_c] \end{cases} \tag{38}$$

$$SAS: \begin{cases} \xi_c(k+1) = \xi_c(k) + 1 & \text{if } m_{count}(k) = 1 \\ \xi_c(k+1) = \xi_c(k) & \text{if } m_{count}(k) = 2 \\ \xi_c(k+1) = 0 & \text{if } m_{count}(k) = 3 \end{cases} \tag{39}$$

$$MS: m_{count}(k) = \begin{cases} 1 & \text{if } \delta_c(k) \wedge \neg\delta_{\xi}(k) \\ 2 & \text{if } \neg\delta_c(k) \wedge \neg\delta_{\xi}(k) \\ 3 & \text{if } \delta_{\xi}(k) \end{cases} \tag{40}$$

We guarantee that an MG cannot be connected to the grid if $\xi_c(k)$ exceeds the maximum number of connections (nc_{max})). Therefore,

$$u_g(k) = 0 \text{ if } \delta_{cmax}(k) = 1 \tag{41}$$

When the timer $\xi_s(k)$ reaches its maximum time period (T_c), the variables $\xi_c(k)$ and $\xi_s(k)$ will be reset, and the binary variable $\delta_c(k)$ will be disabled, allowing the MG to perform nc_{max} grid connections at maximum in the next time period.

3. Optimization problem

In this paper, the proposed dispatch economic problem of an MG is formulated as a short-term, multi-objective optimization problem (i.e., it has a forecasting horizon of up to 6 h [42]). The proposed formulation takes into account not only the battery bank storage levels to be managed by the MG but also the possibility to perform connections to the main grid for selling and purchasing energy. At every instant k, the energy management system must make high-level decisions such as whether to charge or discharge the battery bank, the amount of energy that can be sold or purchased from the main grid, and the loads that can be shifted or disconnected. The mathematical formulation proposed in this paper includes the following constraints:

- Equipment and technologies capacities
- Power flow balance constraints (generation, storage, and demand)
- Maximum amount of grid connections during a determined time interval
- Minimum time intervals that an MG must remain in the grid-connected mode and island mode

The proposed formulation is detailed in the next sections.

3.1. Objective function formulation

The objective function, shown in (42), represents the operational and economic costs of an MG over a planning horizon with N samples. The term $J_{\text{bat}}(k)$ is the operational and maintenance costs of the battery bank, $J_{\text{p}}(k)$ represents the purchase and sale costs of electricity, and $J_{\text{dis}}(k)$ is the discomfort cost for turning off the unexpected loads: $\delta_{\text{crt}}(k)$ is a binary variable that is enabled when the battery bank SOC is lower than its critical level (S_{crt}), and $\delta_{\text{dump}}(k)$ is a binary variable that is enabled when an MG is operating in the island mode, the battery bank is fully charged ($S(k) = 1$), and power generated due to the renewable energy sources is higher than actual demand.

$$J_{\text{N}}(k) = \sum_{i=0}^{N-1} [q_{\text{bat}} J_{\text{bat}}(k+i) + J_{\text{p}}(k+i) + J_{\text{dis}}(k+i) + q_{\text{crt}}\delta_{\text{crt}}(k+i) + q_{\text{dump}}\delta_{\text{dump}}(k+i)] \tag{42}$$

To increase the life cycle of the battery bank, $J_{\text{bat}}(k)$ is penalized by the weight q_{bat} and the critical SOC is penalized by the weight q_{crt}. When the MG is in the island mode and the battery bank SOC is at the maximum level, the excess of RES power generation dissipates in a dump load, wasting energy. The waste of excess renewable power generation is penalized by the weight q_{dump}. The main decisions of the proposed objective function are as follows:

- Minimize the charging and discharging frequency of the battery bank
- Minimize the discomfort caused by unexpected load disconnection
- Maximize the electricity selling while charging the battery bank once the MG is connected to the main grid
- Minimize the waste of the excess RES power generation in the dump load
- Prevent the battery bank from reaching critical SOC to extend its life cycle and ensure the safe operation of the MG

The decision variables of the objective function are the binary variables ($c_{\text{h}}(k)$, $h = 1, \ldots, n_{\text{c}}$) that turn on/off the controllable loads and the operation mode of the MG ($u_{\text{g}}(k)$).

The objective function in (42) is nonlinear because there are multiplications between binary variables and real value functions. By defining some auxiliary variables such as $z(k) = \delta(k)f(k)$, where $\delta(k)$ is a binary variable, we can transform (42) into a linear objective function with the following linear mixed-integer constraints [16]:

$$\begin{aligned} & z \le M\delta \\ & -z \le -m\delta \\ & z \le f(x) - m(1-\delta) \\ & -z \le -f(x) + M(1-\delta) \end{aligned} \tag{43}$$

where f is a real function and M and m are their upper and lower limits respectively. Posteriorly, this transformation is presented according to each objective function term.

3.1.1. Battery bank

The operational and maintenance (O&M) costs of the battery bank (J_{bat}) presented in (44) are related to the charging and discharging frequency of the battery bank. When the MG is in island mode, its charging and discharging frequency depends on the power balance in (25). When the battery bank is not charged and the MG is connected to the grid, the charger of the battery bank is considered a demand load ($D_{\text{c2}}(k)$).

$$\begin{aligned} J_{\text{bat}}(k) = OM_{\text{b}}[\neg u_{\text{g}}(k)[(-2(\delta_{\text{dex}}(k)P_{\text{g}}(k)) + P_{\text{g}}(k)) \\ - \delta_{\text{s2}}(k)D_{\text{c2}}(k)] + \delta_{\text{s2}}(k)D_{\text{c2}}(k)] \end{aligned} \tag{44}$$

In the expression (44), OM_{b} is a cost rate (US$/kWh) and the binary variables satisfy the logical equations (11) and (45).

$$[\delta_{\text{dex}}(k) = 1] \leftrightarrow [P_{\text{g}}(k) < 0] \tag{45}$$

The expressions $\delta_{s2}(k)D_{\text{c2}}(k)$ and $\delta_{\text{dex}}(k)P_{\text{g}}(k)$ are replaced by the following auxiliary variables:

$$\begin{aligned} z_{\text{ch}}(k) &= \delta_{\text{s2}}(k)D_{\text{c2}}(k) \\ z_{\text{dex}}(k) &= \delta_{\text{dex}}(k)P_{\text{g}}(k) \end{aligned} \tag{46}$$

The variable $z_{\text{ch}}(k)$ denotes that the battery bank should be charged when the MG is connected to the main grid and the SOC is no at the maximum level ($\delta_{\text{s2}}(k) = u_{\text{g}}(k) \vee \neg\delta_{\text{s1}}(k)$). The $z_{\text{dex}}(k)$ variable enables the power balance when the RES generation is greater than the load demand. Replacing the auxiliary variables presented in (46) by the respective terms of expression (44), we obtain

$$J_{\text{bat}}(k) = OM_{\text{b}}[\neg u_{\text{g}}(k)[(-2z_{\text{dex}}(k) + P_{\text{g}}(k)) - z_{\text{ch}}(k)] + z_{\text{ch}}(k)] \tag{47}$$

Because there are still nonlinear terms in (47), it is necessary to define another auxiliary variable as follows:

$$z_{bat}(k) = \neg u_{\text{g}}(k)[(-2z_{\text{dex}}(k) + P_{\text{g}}(k)) - z_{\text{ch}}(k)] \tag{48}$$

Finally, replacing $z_{\text{bat}}(k)$ in (47), we have the following linear battery cost:

$$J_{\text{bat}}(k) = OM_{\text{b}}[z_{\text{bat}}(k) + z_{\text{ch}}(k)] \tag{49}$$

Table 1 shows the O&M battery costs for different MG operation modes and power balances, by considering the assumption that the battery bank is not full ($\delta_{\text{s1}}(k) = 0$).

When an MG is isolated, the O&M costs of the battery bank depend on the power balance in (25). When the MG is connected to the grid, the O&M costs depend on the charger demand. All weights of the proposed formulation are equal to or greater than zero. If the power balance is negative ($P_{\text{g}}(k) < 0$), the expression $J_{\text{bat}}(k) = -OM_{\text{b}}P_{\text{g}}(k)$ will always be positive.

3.1.2. Electricity price

In the grid-connected mode ($u_{\text{g}}(k) = 1$), the MG can sell and purchase electricity from/to the main grid. The MG can sell electricity at a selling price $c_{\text{s}}(k)$ when the power balance in (25) is negative. Otherwise, the MG can purchase electricity at a purchasing price $c_{\text{p}}(k)$. The Eq. (50) gives the objective function term representing the purchase and sale of energy:

$$J_{\text{p}}(k) = u_{\text{g}}(k)[(c_{\text{s}}(k) - c_{\text{p}}(k))\delta_{\text{dex}}(k)P_{\text{g}}(k)] + c_{\text{p}}(k)u_{\text{g}}(k)P_{\text{g}}(k) \tag{50}$$

To transform the nonlinear terms of expression (50) in linear terms, we defined the following auxiliary variables:

$$\begin{aligned} z_{\text{p1}}(k) &= (c_{\text{s}}(k) - c_{\text{p}}(k))\delta_{\text{dex}}(k)P_{\text{g}}(k) \\ z_{\text{p2}}(k) &= u_{\text{g}}(k)z_{\text{p1}}(k) \\ z_{\text{bal}}(k) &= c_{\text{p}}(k)u_{\text{g}}(k)P_{\text{g}}(k) \end{aligned} \tag{51}$$

Replacing these auxiliary variables by their respective terms in (50), we obtained the following linear function:

$$J_{\text{p}}(k) = z_{\text{p2}}(k) + z_{\text{bal}}(k) \tag{52}$$

Table 1
O&M battery cost for different MG operation modes and power balances.

Microgrid operation mode	Power balance	J_{bat}
Island ($u_g = 0$)	Positive ($\delta_{dex} = 0$)	$OM_b[P_g - \delta_{s2}D_{c2} + \delta_{s2}D_{c2}] = OM_bP_g$
Island ($u_g = 0$)	Negative ($\delta_{dex} = 1$)	$OM_b[-2P_g + P_g - \delta_{s2}D_{c2} + \delta_{s2}D_{c2}] = -OM_bP_g$
Connected ($u_g = 1$)	Positive ($\delta_{dex} = 0$)	OM_bD_{c2}
Connected ($u_g = 1$)	Negative ($\delta_{dex} = 1$)	OM_bD_{c2}

3.1.3. Controllable loads

In this paper, we considered the demand response program [55], where the customers can specify the curtailment of the controllable loads for better power management. This procedure may occur in critical operation situations; for example, when the MG is isolated and there is low RES power generation. The controllable loads, however, follow the forecasted demand when there is enough power generation. The demand response program usually leads to the user's discomfort, which is represented by a penalty associated with the load curtailment/shedding. The amount of electrical load not met by the MG due to the load curtailment is given by

$$J_{dis}(k) = \sum_{h=1}^{n_c} q_h(1 - c_h(k))D_h \tag{53}$$

where D_h has been defined in (20) and n_c is the total number of controllable electrical loads. The weight q_h penalize the objective function (42) if there is load shutdown.

3.2. Hybrid economic model predictive control

The DHA models of MG presented in Section 2 can be converted to mixed-integer linear inequalities by using the auxiliary variable described in the previous subsection and converting each logical condition $[f(x) \leq 0] \leftrightarrow [\delta = 1]$ to the following inequalities:

$$f(x) \leq M - M\delta \tag{54}$$

$$f(x) \geq \varepsilon + (m - \varepsilon)\delta \tag{55}$$

where ε is an arbitrarily small positive scalar.

Other constraints of MG equipment are related to the upper and lower limits of the SOC, the power balance in (25), and the current balance, see the first three constraints of (56), respectively. The fourth time-varying constraint presented in (56) depends on the demand forecasting curve $D_c^f(k)$. We observed in the last constraint that the generated power is limited by the power forecasting sum of the wind ($P_w^f(k)$) and PV ($P_{pv}^f(k)$) generations.

$$\begin{aligned}
&S_{min} \leq S(k) \leq S_{max}\\
&P_g^{min} \leq P_g(k) \leq P_g^{max}\\
&i_g^{min} \leq i_g(k) \leq i_g^{max}\\
&0 \leq D_c(k) \leq D_c^f(k)\\
&0 \leq P_w(k) + P_{pv}(k) \leq P_w^f(k) + P_{pv}^f(k)
\end{aligned} \tag{56}$$

All constraints containing the real and binary variables can be transformed into a mixed logical dynamical (MLD) system [16], represented by

$$\begin{aligned}
\boldsymbol{x}(k+1) &= \boldsymbol{A}\boldsymbol{x}(k) + \boldsymbol{B}_1\boldsymbol{u}(k) + \boldsymbol{B}_2\boldsymbol{\delta}(k) + \boldsymbol{B}_3\boldsymbol{z}(k)\\
\boldsymbol{y}(k) &= \boldsymbol{C}\boldsymbol{x}(k) + \boldsymbol{D}_1\boldsymbol{u}(k) + \boldsymbol{D}_2\boldsymbol{\delta}(k) + \boldsymbol{D}_3\boldsymbol{z}(k)\\
\boldsymbol{E}_2\boldsymbol{\delta}(k) &+ \boldsymbol{E}_3\boldsymbol{z}(k) \leq \boldsymbol{E}_1\boldsymbol{u}(k) + \boldsymbol{E}_4\boldsymbol{x}(k) + \boldsymbol{E}_5
\end{aligned} \tag{57}$$

where $\boldsymbol{x} = [x_r\ x_b]^T \in R^{v_c} \times \{0,1\}^{v_l}$ are continuous and binary states, $\boldsymbol{u} = [u_r\ u_b]^T \in R^{m_c} \times \{0,1\}^{m_l}$ are continuous and binary inputs, $\boldsymbol{y} = [y_r\ y_b]^T \in R^{p_c} \times \{0,1\}^{p_l}$ are the outputs, $\boldsymbol{\delta} \in \{0,1\}^{r_l}$ and $\boldsymbol{z} \in R^{r_c}$ represent binary and continuous auxiliary variables, respectively.

The proposed HEMPC approach solves the optimal control problem introduced in (58), subject to the MLD constraints in (57) at instant k, given an initial condition $x_0 = x(k)$ and a forecasting horizon N. The optimal solution vector $\mathbf{u}$ contains the controls $u(k), \ldots, u(k+N-1)$; however, with the receding horizon principle, we applied only $u(k)$ and abandoned the remaining control actions. In the next sample $k+1$, we updated the initial conditions $x_0 = x(k+1)$ and calculated a new sequence of control actions $u(k+1), \ldots, u(k+N)$. This procedure is repeated in real time until the planning horizon N_p is reached.

$$P_N = \min_u J_N(k)(\mathbf{x}, \mathbf{u}, \boldsymbol{\delta}, \boldsymbol{z}) \tag{58}$$

Fig. 2 outlines the proposed economic dispatch procedure. First of all, the HEMPC receives the electricity prices ($c_s(k)$ and $c_p(k)$), wind speed ($\upsilon(k)$), irradiance ($\lambda(k)$), temperature ($T(k)$), and load demand forecasts ($D(k)$). The wind power generation is calculated from the wind turbine MLD model presented in the Eqs. (7)–(10) and the PV power generation is determined from the PV MLD model in (3), (4), and (5). The HEMPC also receives the objective function penalties and the initial condition x_0. Next, the receding horizon strategy is applied at each sample time T_s with the new measured/estimated states $\boldsymbol{x}(k+1|k+1) = \boldsymbol{x}_{k+1}$. By doing so, a feedback policy is designed.

Table 2
Microgrid equipment specifications.

Microgrid equipment	
PV Panels	Six PV panels of 250 Wp each, total power: 1500 Wp, open circuit voltage: 37.8 V, short circuit current: 8.71A, Axitec, model: AC-250P/156-60S [56]
PV inverter	Power: 2.0 kW, output voltage: 220 V, Fronius, model: Fronius Galvo 1.1-5 [57]
Wind turbine	2.46 m blade diameter wind generator, nominal power: 1000 W, output voltage: 220 V, cut-in wind speed: 2 m/s, nominal wind speed: 11 m/s, cut-off wind speed: 16 m/s, Enersud, model: GERAR246 [58]
Wind inverter	Power: 1,5 kW, output voltage: 220 V, Ginlong, model: CO.LTD GCI-1.5kW [59]
Energy storage system	Eight lead–acid batteries, 12 Vdc, 55 AH, Moura, model: 12MF55 [60]
Resistive loads	Six resistors with 500 W each, 127 V, Denktherm, model: BR6-500/127

4. Numeric results

The proposed predictive control algorithm was applied to an MG composed of photovoltaic panels, wind turbine, converters (PV and wind converters), charge control panel, controllable loads, battery bank for energy storage, and a common connections panel (see Fig. 3) Table 2 presents the characteristics of the equipment used in all numeric results.

The proposed algorithm was implemented using MATLAB with CPLEX and HYSDEL toolboxes. The computer used has Intel Core i7-7700 3.6 Ghz processor, 16 Gb RAM, Linux Ubuntu 18.10 64 bits. We have analyzed the HEMPC performance for two simulation scenarios:

1. Scenario 1: Prioritizes battery bank conservation through the q_{bat} penalty in (42)
2. Scenario 2: Prioritizes energy sales by decreasing the q_{bat} value by 10 times compared to Scenario 1

Moreover, the proposed scenarios should minimize the purchased energy, the waste of renewable energy and the shutdown of loads, allowing the MG to continue offering services to the main grid and meeting the user demand.

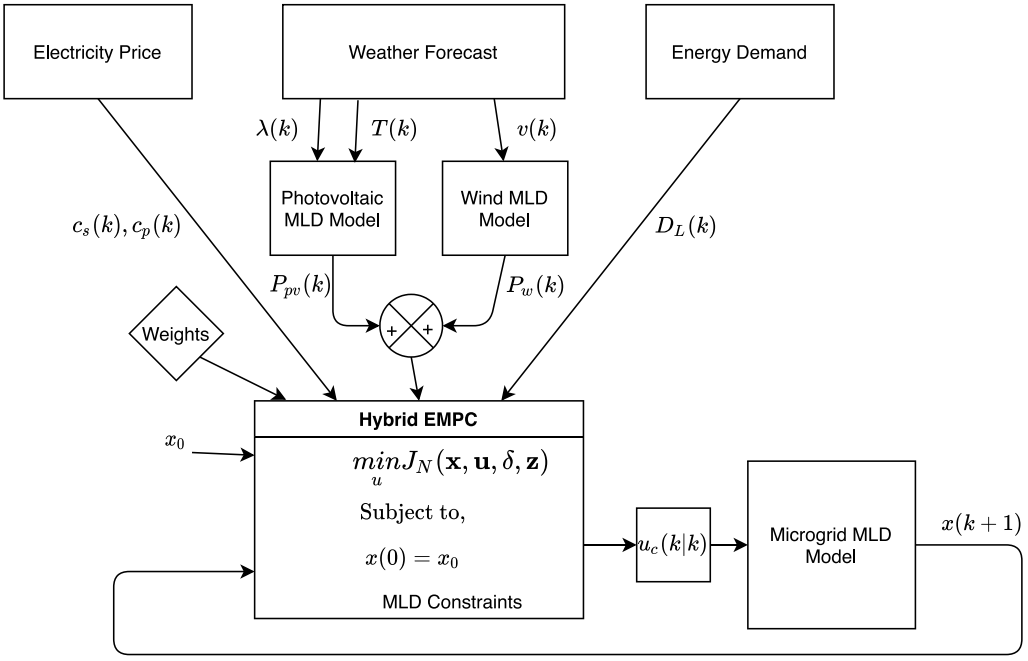

Fig. 2. Hybrid EMPC block diagram.

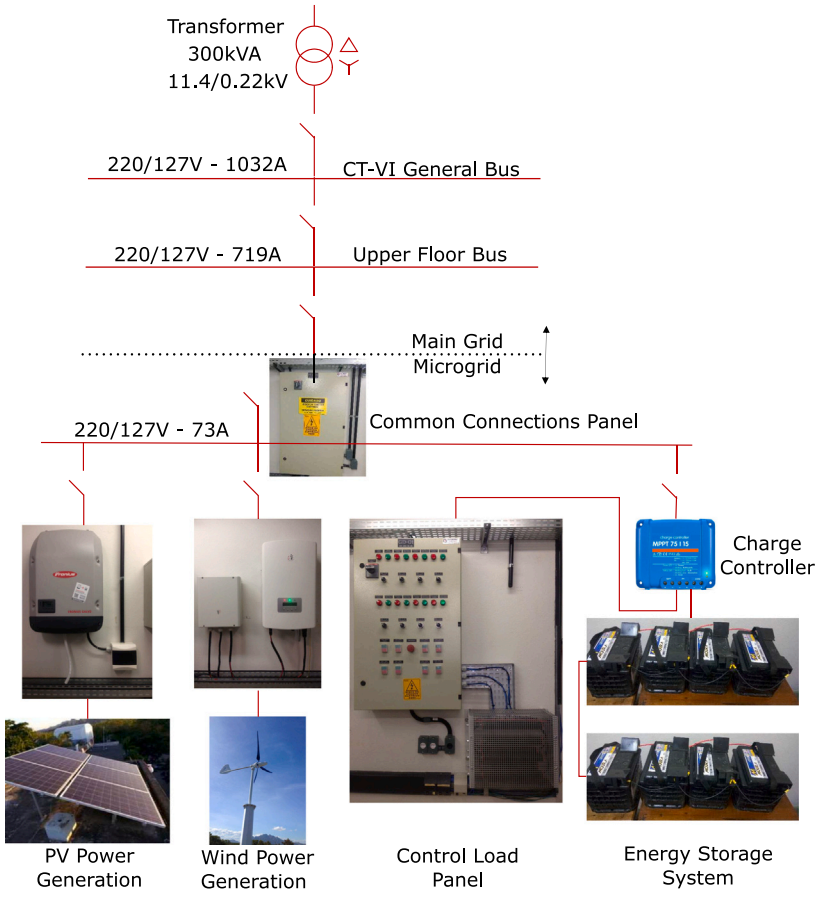

Fig. 3. Single-line diagram of the microgrid and its connection to the main grid.

Table 3
Common parameters for all scenarios.

Parameters	Value	Unit
i_{ch}	3.5	A
N	1	h
N_p	168	h
η	0.95	pu
OM_b	0.08	US$/kWh
P_g^{min}	−2.5	kW
P_g^{max}	2.5	kW
S_{min}	0.0	pu
S_{max}	1.0	pu
S_{crt}	0.5	pu
T_s	10	min

The performance analysis of the proposed control algorithm is carried out through simulations using real weather data and forecasts. The weather data of irradiance, temperature, and wind speed were extracted from the National Institute of Meteorology [61]. We used the weather research and forecasting (WRF) model [44] for estimations of the direction and speed of wind, air temperature, and global radiation. The model consists of four telescoping nests, with horizontal resolutions of 27 km on the outermost domain (d01), 9 km on the first nest (d02), 3 km on the second nest (d03), and 1 km on the innermost nest (d04). The numerical grid was configured with 31 vertical levels that follow the terrain, with the first six levels at approximately 25 m, 58 m, 74 m, 89 m, 110 m, and 141 m above the ground. The WRF model starts automatically every day at 2:00 a.m. (local time), using the boundary conditions data of the Global Forecast System [62]. The model runs twice, generating meteorological forecasts within a horizon of 24 h and with a resolution of 10 min (i.e., $10, 20, 30 \ldots 1440$ min), for Natal [20.19^oS and 40.2^o W], and Santa Vitoria do Palmar [33.742297^o S and 53.37221^o W]. The locations may be briefly described as follows:

(1) Natal-RN. Located in the northeast of Brazil, it has a hot and humid climate with average temperatures around 28 ^{o}C and average wind speed of 3.4 m/s. In Natal, the summer is hot and partly cloudy; the winter is short and warm and with an almost cloudless sky. During the whole year, precipitation and medium to strong wind occur. The average irradiance is 248 W/m^2.
(2) Santa Vitoria do Palmar-RS, Brazil. Located in the extreme south of Brazil, on the border with Uruguay. It has a mild climate with average temperatures around 18^oC. It has an average wind speed of over 6.5 m/s, which is considered a good average for installing wind turbines. In Santa Vitoria do Palmar, the summer is warm and muggy; the winter is mild. During the whole year there is precipitation and strong wind with partly cloudy skies.

Table 3 shows the common parameters used for all simulation scenarios. The current value $i_{ch}(k)$ of the battery bank is within a range defined in [60] to obtain the highest charging and discharging efficiency. We chose the forecasting horizon (N) to guarantee the lowest computational cost without compromising the stability of the HEMPC. We tested all the MG's operations with a planning horizon (N_p) of one week. According to [42], this period is adequate to evaluate the performance of the management algorithm because the weather data used in the simulation have different characteristics. The charge and discharge efficiencies of the battery bank are equal to 0.95, see [31]. The O&M cost of the battery bank was estimated from its total cost specified in Table 2, divided by the lifetime. The critical SOC is based on the manufacturer's recommendations to keep the discharge variation as smooth as possible in order to increase the battery life.

We chose the objective function penalties presented in Table 4 according to the priority established for each simulation scenario. Scenario 2 prioritizes the sale of energy, and it has the lowest q_{bat} parameter in relation to the other scenarios. The penalties $q_2 \cdots q_5$ refer to the controlled loads by contactors $c_2 \cdots c_5$ shown in (53). In

Table 4
Numerical values of objective function weights for each Scenario.

Parameters	Scenario 1	Scenario 2
q_{bat}	1	0.1
q_2	0.01	0.01
q_3	20	0.01
q_4	0.01	0.01
q_5	0.01	0.01
q_{crt}	100	100
q_{dump}	50	50

Table 5
Parameter values of the MG grid-connection constraints for each weather station.

Parameters	Santa vitoria	Natal	Unit
nc_{max}	3	5	–
T_{down}	4	5	Samples
T_{up}	5	6	Samples
T_c	144	144	Samples

Scenario 1, load 3 has the highest priority to remain connected, and in Scenario 2, the loads have the same priority. The value of q_{crt} is high to prevent the SOC level of the battery bank from exceeding its critical value; whereas, q_{dump} is high to reduce the waste of excess renewable generation.

Table 5 shows the parameter values related to the MG grid-connection constraints nc_{max}, T_{down}, T_{up}, T_c for each weather station situated in different geographical locations. The transients for MG converters must respect the minimum time of 300 s [63]. Therefore, the minimal time intervals τ_c and τ_i in (26) and (27) respectively must be greater than such value specified in the standard.

Fig. 4 presents the daily curves of the energy purchase and sale prices. Note that the energy sale price is most attractive between midday and 3:00 p.m.. The purchase price of energy increases at peak hours between 5:00 p.m. and 10:00 p.m..

The power demand of the MG has a characteristic similar to that of a typical residence, where there are turn on or turn off controllable loads and a critical load of ($D_1 = 0.25$ kW) that remains always turned on. Demand for controllable loads is presented in (59). Such loads can be turned off at any time by the controller, thus generating a met demand.

$$\begin{aligned} &[c_2(k) = 1] \leftrightarrow [D_2 = 0.15 \text{ kW}] \\ &[c_3(k) = 1] \leftrightarrow [D_3 = 0.20 \text{ kW}] \\ &[c_4(k) = 1] \leftrightarrow [D_4 = 0.20 \text{ kW}] \\ &[c_5(k) = 1] \leftrightarrow [D_5 = 0.30 \text{ kW}] \end{aligned} \tag{59}$$

We evaluated the proposed algorithm performance by defining the user comfort index (CI) through the following equation:

$$CI = \frac{D_L^m}{D_L^r} 100 \ \% \tag{60}$$

where D_L^m is the average met demand and D_L^r is the average real demand during the planning horizon.

The met demand differs from the real demand when the MG management algorithm removes loads to minimize operating costs. The forecasted demand ($D_L^f(k)$) can be scheduled in advance and unpredictable loads can be shedding to the forecasted demand before applying the optimization algorithm, providing the real demand. We also assumed that the real demand shifts over time in relation to the forecasted demand and the forecasting error is around 10% (see Fig. 5).

Fig. 6(a) shows the time series of real and forecasted temperatures over a week at the Santa Vitoria-RS weather station. The average temperature is equal to 19.34 ^{o}C, and the minimum and maximum temperatures are equal to 12 ^{o}C and 26 ^{o}C, respectively. Fig. 6(b) shows the time series of the temperature forecasting error, in which the mean absolute error (MAE) and mean relative error (MAPE) are equal to 1.51 ^{o}C and 7.81% respectively.

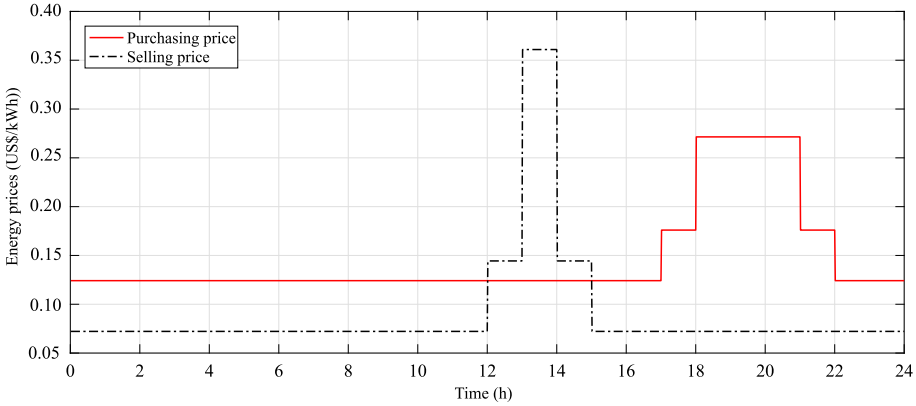

Fig. 4. Energy prices over 24 h.

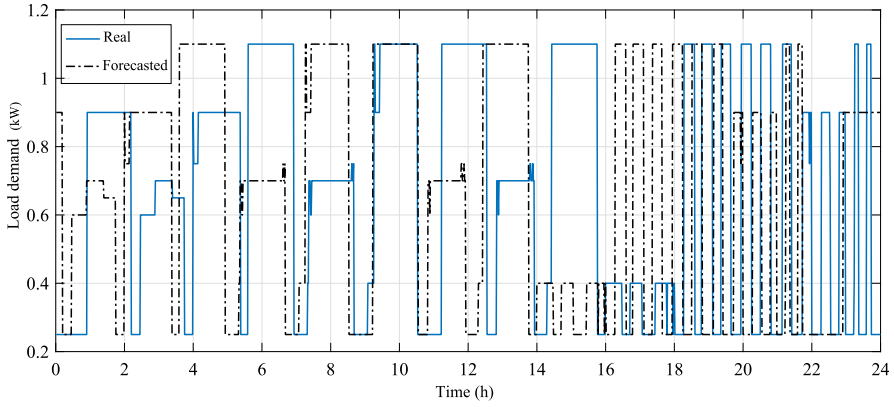

Fig. 5. Real and forecasted demand curves over 24 h.

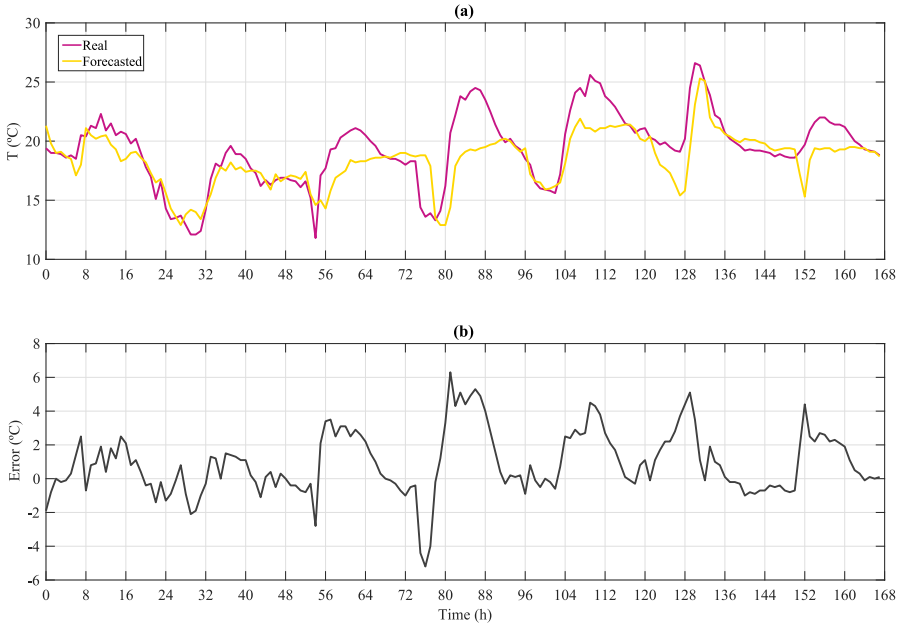

Fig. 6. (a) Temperature curves; (b) Temperature forecasting error over one week.

Fig. 7(a) shows the time series of real and predicted irradiance collected during one week at the Santa Vitoria-RS station. In this case, irradiance has its peak range between 7:00 a.m. and 6:00 p.m., with an average around 264.0 W/m^2. Fig. 7(b) shows the curve of the irradiance forecasting error, with MAE and MAPE equal to 60.0 W/m^2 and 22.83%, respectively.

Fig. 8(a) shows the wind speed profile observed at Santa Vitoria station for a week. The average wind speed is 6.71 m/s and there are

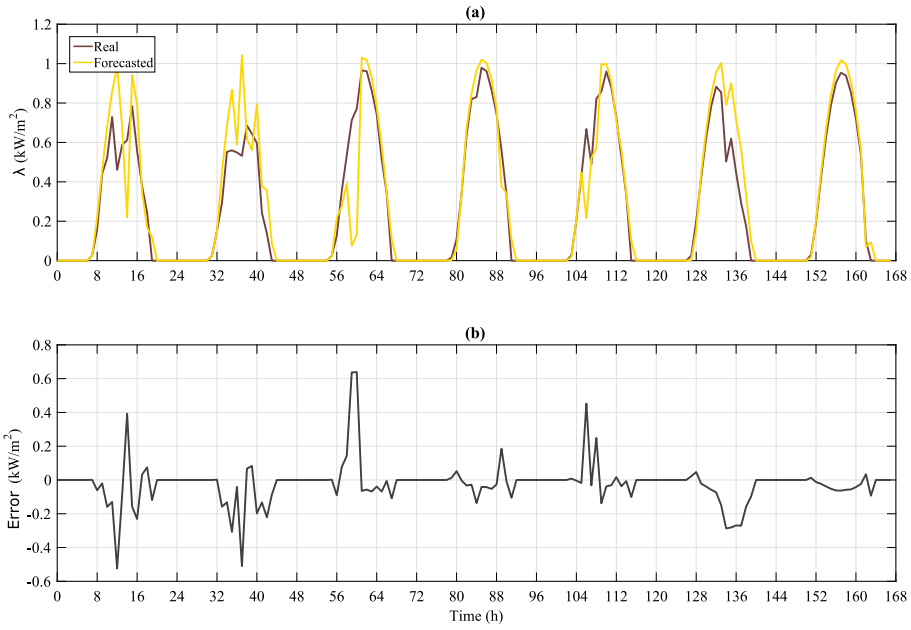

Fig. 7. (a) Irradiance curves; (b) Irradiance forecasting error over one week.

gusts greater than 15 m/s. Fig. 8(b) shows the wind speed forecasting error curve, with MAE of 1.78 m/s and MAPE of 26.60%.

The weather data forecasts obtained from the WRF model were converted to photovoltaic and wind power forecasts through the mathematical models presented in Sections 2.1 and 2.2, respectively. Because of the difference in heights between the weather station and the wind turbine, we recalculated the real wind in the turbine from an extrapolation technique (see Appendix A).

Table 6 shows low correlation coefficient between the forecasting errors of renewable power and weather data obtained from the Santa Vitoria-RS and Natal-RN stations.

Thus, we observed from the statistics presented in Tables 7 and 8, that the forecast errors of the photovoltaic and wind power are worse than the forecast errors of the weather data.

Next, we discuss the results obtained for each scenario, considering that the weather data forecasts are determined from the WRF model. Fig. 9(a) shows the evolution of the battery SOC and the MG connection mode for Scenario 1 in Santa Vitoria do Palmar during a week of operation. Fig. 9(b) shows that Eq. (25) is satisfied because the power balance is negative when there is an excess of energy production. In the case of low energy generation, the balance tends to be positive or close to the origin of the graph. In the first 72 h there is a large amount of renewable power, as shown in Fig. 9(b), that keeps the battery SOC at its maximum level during most of this period. When the SOC reaches its maximum value, there is no charging and discharging of the battery bank in such a way that there is a lower O&M cost.

In addition, the MG sells energy during most of the first 72 h because the energy balance, as shown in Fig. 9(b), is negative. Between the 4th and 6th days (or 72 h and 144 h), there is a low amount of renewable energy generation, which makes the MG connect to the main grid to buy energy and prevent the battery bank from reaching its critical SOC. From the end of the 6th day onwards, we observed an adequate renewable generation. In addition, the SOC level increases because the MG connects to the grid to sell the excess renewable energy, avoiding having to dissipate it in the dump load. We observed that the proposed optimization algorithm does not violate the maximum number of connections or the minimum time that the MG must remain connected to the main grid.

Fig. 10 shows the real and met demands associated with the simulation presented in Fig. 9. Note that the met-demand curve follows the real-demand curve, indicating that the HEMPC experiences a low level of load shedding.

Fig. 11 shows the simulation result for Scenario 2 in Santa Vitoria do Palmar. In this scenario, the MG remains connected to the grid for a longer time than in Scenario 1. Thus, the battery SOC shown in Fig. 11(a) remains at its maximum value for about 63 h. Consequently, the MG sells more energy than it does in Scenario 1, but it also buys more energy when the power balance, shown in Fig. 11(b), becomes positive. In addition, the power balance presents a smoother oscillation than in Scenario 1, between the 4th and 6th days (72 h and 144 h), thus producing little renewable energy.

Fig. 12 shows the profiles of the real and met demands. The met demand has a behavior similar to that in Scenario 1, where the HEMPC algorithm almost does not shutdown loads.

4.1. Sensitivity analysis of the HEMPC algorithm in relation to the forecasting errors

This analysis is carried out with respect to the comfort index (CI), cost of the battery bank, profit from energy sale, cost of purchased energy, and the cost of waste of renewable energy. These last four terms are defined as follows:

$$C_{\text{bat}} = \sum_{k=1}^{N_p} J_{\text{bat}}(k) \tag{61}$$

$$J_s = \sum_{k=1}^{N_p} c_s(k) P_g(k), \text{ when } u_g(k) = 1 \text{ and } \delta_g(k) = 0 \tag{62}$$

$$J_{\text{pur}} = \sum_{k=1}^{N_p} c_p(k) P_g(k), \text{ when } u_g(k) = 1 \text{ and } \delta_g(k) = 1 \tag{63}$$

$$J_{\text{dump}} = \sum_{k=1}^{N_p} c_s(k) P_g(k), \text{ when } \delta_{\text{dump}}(k) = 1 \tag{64}$$

In addition, we defined financial profit through the following expression:

$$profit = J_s - J_{\text{pur}} - J_{\text{dump}} \tag{65}$$

Table 6
Correlation coefficients between power and weather data.

	PV power errors and temperature errors	PV power errors and irradiance errors	Wind power errors and wind speed errors
Santa Vitoria	0.03	0.71	0.64
Natal	0.14	0.53	0.65

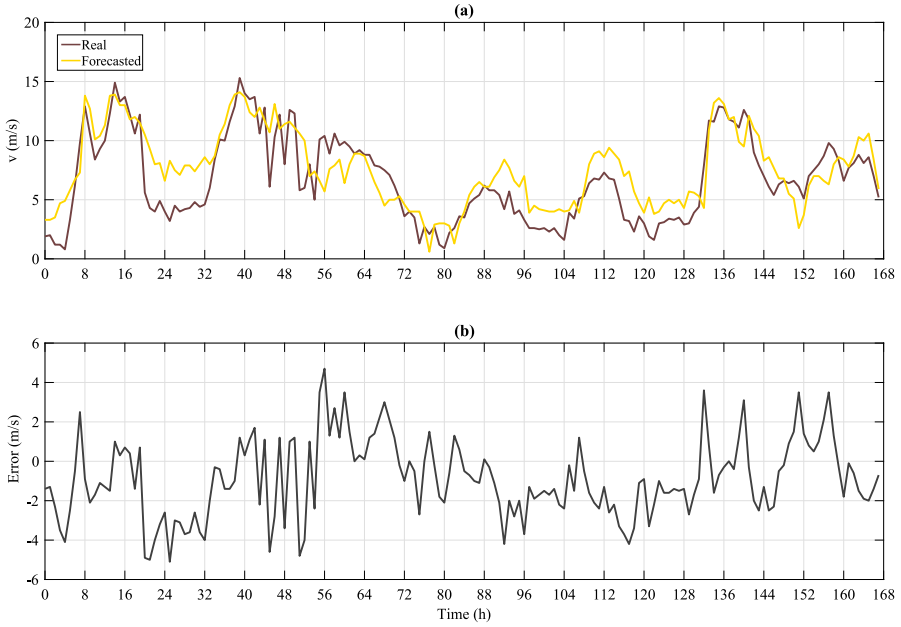

Fig. 8. (a) Wind speed curves; (b) Wind forecasting error over one week.

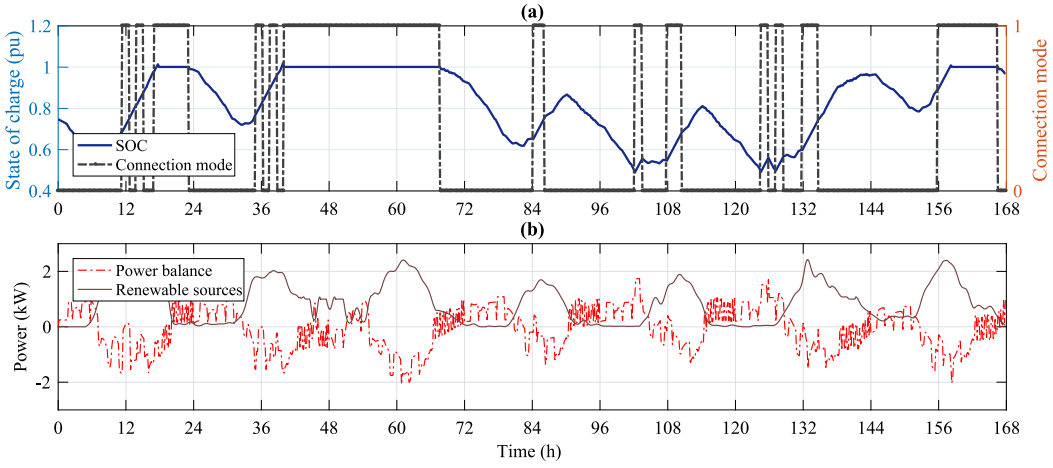

Fig. 9. Scenario 1: (a) State of charge and connection mode of MG; (b) Power balance and RES power over one week.

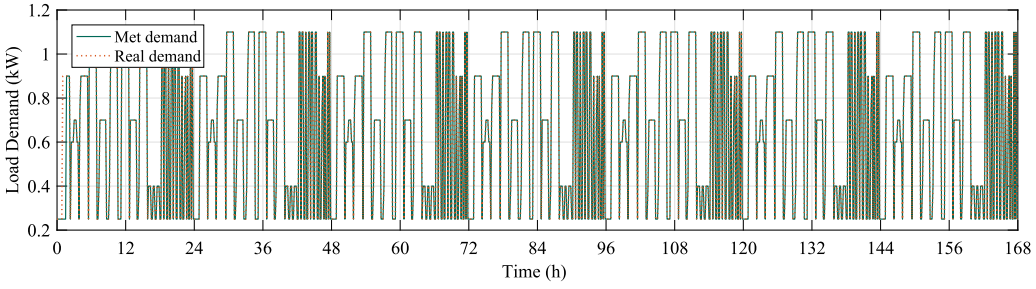

Fig. 10. Scenario 1: Real and met demands over one week.

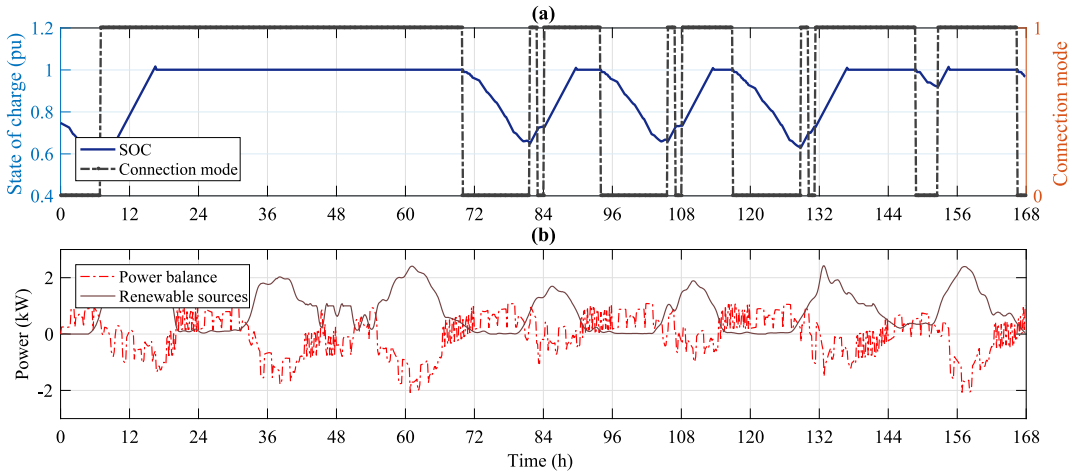

Fig. 11. Scenario 2: (a) State of charge and connection mode of MG; (b) Power balance and RES powers over one week.

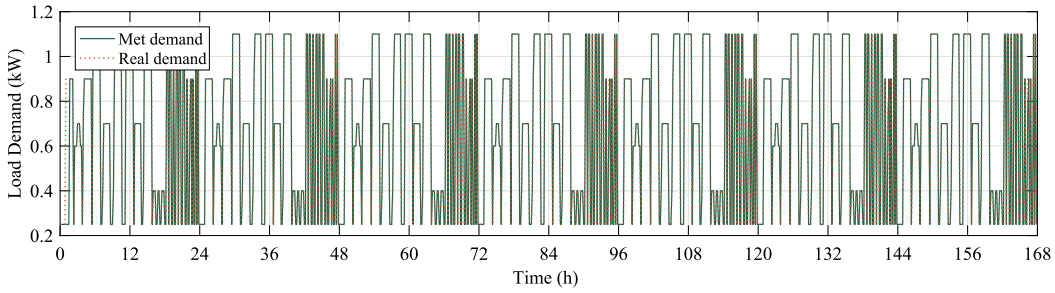

Fig. 12. Scenario 2: Real and met demands over one week.

Table 7
Statistic values of renewable power and weather forecasting errors at Santa Vitoria-RS.

Santa Vitoria-RS		Mean	MAE	MAPE (%)
Power	Photovoltaic	388.4 W	93.9 W	24.17
	Wind	482.0 W	248.6 W	51.58
Weather data	Temperature	19.31 °C	1.51 °C	7.81
	Irradiance	264.0 W/m^2	60.0 W/m^2	22.83
	Wind speed	6.71 m/s	1.78 m/s	26.60

Table 8
Statistic values of renewable power and weather forecasting errors at Natal-RN.

Natal-RN		Mean	MAE	MAPE (%)
Power	Photovoltaic	399.4 W	96.8 W	24.22
	Wind	96.7 W	67.3 W	69.58
Weather data	Temperature	28.31 °C	1.08 °C	3.82
	Irradiance	272.0 W/m^2	62.0 W/m^2	22.61
	Wind speed	3.32 m/s	0.95 m/s	28.54

To assess the impact of the weather and load scheduling forecasting errors on the proposed HEMPC algorithm, we defined the following forecasting strategies:

F1: Forecast of weather data using WRF with forecast error of the load schedule, applying a 2-hour shift (related to the real load) to the expected load

F2: Forecast of weather data using WRF with perfect forecast (without error) of the load scheduling

F3: Perfect forecast in weather data and perfect load scheduling

The HEMPC algorithm with the forecast strategy F3 is deterministic and it is considered as a benchmark. Table 9 shows that the MG needs to buy energy in all scenarios, considering all forecasting strategies evaluated by the HEMPC. Because there is not enough wind generation in Natal, we observed that more energy is purchased in order not to violate the critical SOC and impair the lifespan of the battery bank. In addition, considering all HEMPC scenarios and forecasting strategies, both in Natal and Santa Vitoria, a high level of comfort is observed (less than 1% of demand is not met), and there is no waste of energy due to excess of renewable generation. Regarding the Natal weather station, we observed, for each scenario (1 and 2), that the terms C_{bat}, J_s and J_{pur} do not vary considerably when we modify the forecasting strategy. Therefore, the HEMPC algorithm is not highly sensitive to forecasting errors, which can eventually happen due to low generation of wind energy in Natal.

However, because appropriate solar energy production was combined with excellent wind energy production from the Santa Vitoria do Palmar station, we observed (see Table 9) that when applied to this location, the proposed optimization algorithm has financial profit, and the battery bank operation average cost is 39.6% lower than it is in Natal-RN. Unlike Natal, where the MG connects to the main grid to avoid overtaking the critical SOC, the grid connection in Santa Vitoria enables the excess of generated energy to be sold because the batteries remain charged for a long period, as shown in Fig. 11. In Santa Vitoria, the indexes analyzed in Table 9 have greater variations when the three HEMPC forecasting strategies are compared. In addition, the perfect forecast (F3) achieves 19.5% more profit, on average, than the F2 forecasting strategy, which cost the battery bank 27.4% more.

Therefore, we have concluded that the proposed algorithm is more sensitive to forecasting errors when there is a considerable amount of renewable energy production, where such errors substantially affect the cost of the battery bank as well as the financial profit (27.3% for the former and 13.3% for the latter), whereas there is a minor degree of variation in terms of comfort index (less than 1%).

Table 9
Sensitivity analysis with respect to the forecasting errors for Scenarios 1 and 2 over one week.

Location	Scenarios	Forecast	C_{bat} (US$)	J_s (US$)	J_{pur} (US$)	J_{dump} (US$)	profit (US$)	CI (%)
Natal Brazil	1	F1	6.91	0.20	6.38	0.00	−6.18	100.00
		F2	6.89	0.20	6.44	0.00	−6.24	100.00
		F3	6.76	0.19	6.59	0.00	−6.40	100.00
	2	F1	7.19	0.41	5.20	0.00	−4.79	99.56
		F2	7.18	0.41	5.20	0.00	−4.79	99.56
		F3	6.99	0.44	6.13	0.00	−5.69	99.93
Santa Vitoria Brazil	1	F1	5.44	4.48	1.50	0.00	2.98	99.37
		F2	5.24	4.73	1.65	0.00	3.08	99.56
		F3	6.08	4.36	1.01	0.00	3.35	99.56
	2	F1	4.10	6.65	2.44	0.00	4.21	99.56
		F2	3.77	6.84	3.09	0.00	3.75	99.56
		F3	5.39	6.00	1.20	0.00	4.80	99.56

Table 10
Comparison of battery cost, financial profit and comfort index among the HEMPC, MILPm and RBS strategies.

Location	Scenarios	Strategy	C_{bat} (US$)	J_s (US$)	J_{pur} (US$)	J_{dump} (US$)	profit (US$)	CI (%)
Natal Brazil	1	RBS	6.82	0.25	4.70	0.00	−4.45	92.52
		MILPm	8.50	0.01	5.63	0.00	−5.62	100.00
		HEMPC	7.37	0.17	5.63	0.00	−5.46	99.57
	2	RBS	5.80	0.18	3.61	0.01	−3.44	80.26
		MILPm	7.29	0.40	7.51	0.68	−7.79	100.00
		HEMPC	7.71	0.34	4.35	0.00	−4.01	99.61
Santa Vitoria Brazil	1	RBS	6.53	1.58	0.33	1.92	−0.67	94.69
		MILPm	7.35	0.42	2.42	2.26	−4.26	99.92
		HEMPC	6.46	4.70	0.62	0.01	4.07	99.91
	2	RBS	6.08	1.85	0.18	2.14	−0.47	89.15
		MILPm	4.93	1.25	4.97	3.48	−7.20	100.00
		HEMPC	4.96	6.74	2.01	0.00	4.73	99.93

4.2. Comparison of the proposed algorithm with others MG management strategies.

In this section the performance of the HEMPC strategy has been compared with the following MG management techniques:

Rule-based strategy (RBS): It mimics the logical decision of an MG operator. The description of this algorithm can be found in Appendix B

MILP multi-period (MILPm): It consists in the solution of successive MILP problems (42) with a 6-hour forecasting horizon until reaching the planning horizon of 168 h. The proposed strategy solves the MILP problem at a sampling rate of 10 min, and the data update occurs every 6 h. A longer forecasting horizon would lead to the overflow of computational memory

The HEMPC and MILP multi-period are receding horizon strategies; however, the HEMPC updates the meteorological data for each sampling period and applies the first solution obtained from the MILP problem in the management of the MG (closed-loop strategy). In MILPm, the data update occurs at multiple times of the forecasting horizon after the resolution of each MILP problem, and we use all calculated solutions in the MG management open loop or myopic strategy [64]).

Figs. 13(a) and 14(a) show the SOC levels of Natal and Santa Vitoria, respectively, for Scenario 1. Note that, because of the low generation in Natal, the SOC oscillates around the critical level (S_{crt} = 0.5) for the MILPm and RBS strategies and above the critical level for the HEMPC. Because of the high generation in Santa Vitoria, the HEMPC and RBS operate above the critical SOC, and MILPm violates the critical SOC only at the beginning of the simulation. Figs. 13(b) and 14(b) show the energy balances in Natal and Santa Vitoria, respectively.

Table 11
Comparison of MG operational safety indexes among the HEMPC, MILPm and RBS strategies.

Location	Scenarios	Strategy	SOC_{min}	T_{crt} (min)	PT_{crt} (%)
Natal Brazil	1	RBS	0.38	710	7.04
		MILPm	0.32	4380	43.45
		HEMPC	0.49	110	1.09
	2	RBS	0.49	210	2.08
		MILPm	0.43	210	2.08
		HEMPC	0.49	70	0.69
Santa Vitoria Brazil	1	RBS	0.49	20	0.20
		MILPm	0.30	530	5.26
		HEMPC	0.49	20	0.20
	2	RBS	0.54	0	0.00
		MILPm	0.46	100	0.99
		HEMPC	0.53	0	0.00

Note that the energy balance is predominantly positive in Natal and predominantly negative in Santa Vitoria (i.e., there is more energy being sold in Santa Vitoria and more energy being purchased in Natal). We confirmed this from Table 10, which shows that all strategies had an economic loss in Natal, and only the HEMPC makes a profit in Santa Vitoria. This is because the MILPm and RBS strategies in Santa Vitoria wasted the excess renewable energy, instead of selling it, causing losses. Also, Table 10 shows that the demand comfort index (CI) of RBS was below 94.69%, whereas MILPm and the HEMPC had a CI higher than 99% in all scenarios (MILPm had an average CI index 0.3% higher than the HEMPC and 13% greater than RBS). Although RBS has a lower CI index, its battery cost in Natal was the smallest (i.e., RBS prefers to discard load to conserve the battery when low power generation occurs). However, in Santa Vitoria, the average battery cost of the

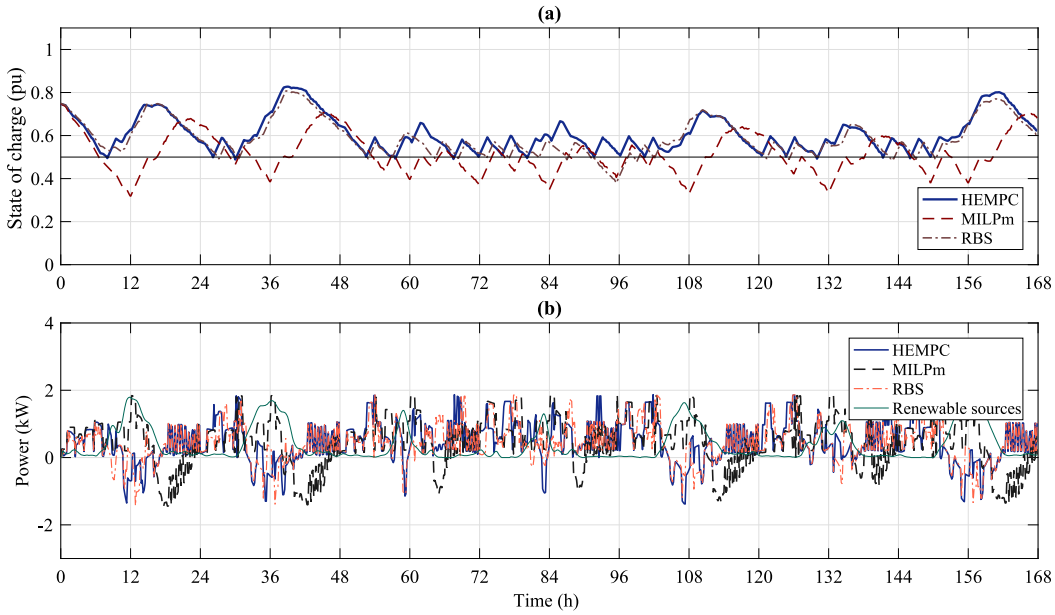

Fig. 13. Comparison of the MG management strategies for Natal: (a) SOC levels and (b) Power balances and RES powers.

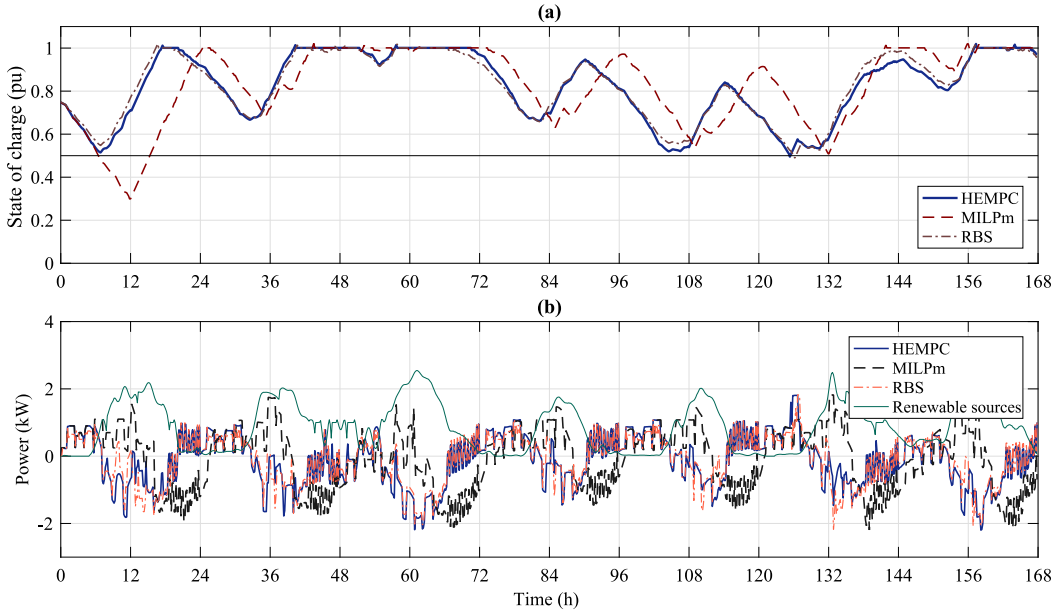

Fig. 14. Comparison of the MG management strategies for Santa Vitoria: (a) SOC levels and (b) Power balances and RES powers.

Table 12
Computational cost between iterations for different prediction horizons.

N (h)	Number of decision variables	Number of constraints	Average times (s)	Worst case times (s)	Memory (MB)
1	42	552	3.4	3.6	507
3	126	1656	3.5	3.7	521
6	252	3312	11.1	11.4	565

HEMPC was lower than that of the other strategies (for RBS, the average battery cost was 10.3% higher than the HEMPC and for MILPm it was 7.5% higher). Therefore, MG management from the HEMPC in scenarios with higher power generation is the most economically efficient.

Table 11 compares the MG security indexes defined by the minimum SOC ($S_{\min}$) obtained from the battery bank during the simulation period, the time period (T_{crt}) during which the SOC was below the critical SOC, and the percentage rate (PT_{crt}) between T_{crt} and the total simulation time. Through this table, we noticed that the SOC level furnished by MILPm reached values lower than the critical SOC over a long time, mainly in low power generation. Thus, the MILPm strategy has a higher operational risk because the battery operation at low levels over a long period decreases the reliability of the MG operation. In contrast, we observed that for the HEMPC, the minimum SOC level was close to 0.5, and the average T_{crt} is 90 min in Natal and 10 min in Santa Vitoria (PT_{crt} equal to 1.4% and 0.1%, respectively). Therefore, the HEMPC is safer in any scenario because the SOC levels furnished

by MILPm and RBS stay below the critical SOC during a period 19.7 times and 4.3 times greater than the HEMPC, respectively.

4.3. Computational complexity

The HEMPC solution, made through the MILP model, requires a computational time proportional to the forecasting horizon. As shown in Table 12, the computational time to solve the optimization problem for horizons less than or equal to 6 h is considerably lower than the sampling rate (10 min or 600 s). We do not recommend forecasting horizons larger than 6 h because the computational time to solve the MILP problem increases considerably and there may be a memory overflow due to the large number of decision variables and constraints. Therefore, there will not be much time left for the algorithm to perform predictions during the 10 min sampling period. Moreover, the solutions obtained by the HEMPC with forecasting horizons from one to 6 h converged to near values in all tested meteorological scenarios and for different forecasting strategies without presenting infeasibilities.

5. Conclusion

This paper presented a new optimization model for microgrid management from the hybrid economic model predictive control strategy using weather forecasts by the global model. The proposed optimization algorithm has autonomy in decision-making to perform connection/disconnection with the main grid to provide ancillary services, such as the sale of excess power generation. This service helps the main grid in the power supply for its demand when the selling price of energy is advantageous and the microgrid has excess power generation. Moreover, the model considers a maximum limit of grid-connection occurrence, and after the microgrid connects to the main grid, it must remain connected for a minimum time interval. These constraints give flexibility to adapt the microgrid control algorithm to various grid-connection policies established by the power utility. The proposed optimization algorithm can be applied in any location and does not depend on the physical installations of surface meteorological stations. It can be used for feasibility studies in any location based on the geographic coordinates of the future installation of a microgrid and its equipment specifications.

The performance of the proposed control algorithm was analyzed through simulations using real weather data with different meteorological characteristics. The real demand is shifted over time, leading to a demand forecasting error of 10%. Using the weather data forecasts, the new hybrid wind and solar power generation models presented high forecasting errors that caused variations in the optimization results of 1% in the met demand, 27.3% in the battery bank costs, and 13.3% in the financial profits. A comparison among different management strategies showed that multi-period mixed integer linear programming and the proposed algorithm had a demand comfort index of over 99% in all scenarios, whereas the ruled-based strategy was less than 94.7%. Moreover, multi-period mixed integer linear programming and the ruled-based strategy had state of charge of the battery bank below the critical state of charge during a period 19.7 and 4.3 times higher than that furnished by the proposed algorithm, respectively. Thus, in terms of the microgrid operational safety, the hybrid economic model predictive control is more efficient in all scenarios. In the low energy-generation scenario, all management policies showed losses with the sale of energy. In the situation with high energy generation, only the proposed strategy showed a profit. Besides, the ruled-based and multi-period mixed integer linear programming strategies had an average battery cost of 10.3% and 7.5% higher than the hybrid economic model predictive control did, respectively. Therefore, in locations with high energy generation, the proposed algorithm is more economically advantageous.

Although solutions to optimization problems using hybrid models require a high computational cost, the results of the proposed algorithm remained stable over the planning horizon with forecasting horizons between 1 and 6 h. Moreover, the results showed that real-time optimization is feasible with sampling periods of up to 10 min. Future work suggests implementing the proposed framework in a real plant considering the control loops of the converters, battery bank charger, and a formal controller stability analysis.

Nomenclature

	Abbreviations
DHA	Discrete Hybrid Automata
EG	Event Generator
EMS	Energy Management System
ESS	Energy Storage System
FSM	Finite State Machine
HEMPC	Hybrid Economic Model Predictive Control
HMPC	Hybrid Model Predictive Control
MILP	Mixed Integer linear Programing
MG	Microgrid
MLD	Mixed Logic Dynamic
MPC	Model Predictive Control
MPPT	Maximum Power Point Tracking
MS	Mode Selector
O&M	Operation and Maintenance
PV	Photovoltaic
RBS	Rule Based Strategy
RES	Renewable Energy Resources
SAS	Switch Affine System
SOC	State of Charge
WRF	Weather Research and Forecasting
	Parameters
η	Storage charging and discharging efficiencies
A	Ideality factor
a_{n}	Wind turbine polynomial coefficients
$C_{\max}$	Storage capacity [Ah]
d_n	Photovoltaic panel polynomial coefficients
I_{sc}	Short-circuit current [A]
k	Time instant [s]
k_B	Boltzmann constant [$\mathrm{m^2kgs^{-2}K^{-1}}$]
n_{c}	Number of controllable loads
n_l	Number of critical loads
$nc_{\max}$	Maximum number of grid-connections
N	Prediction Horizon [h]
N_{p}	Scheduling Horizon [h]
OM_{b}	O&M costs of battery bank [R$/ kWh]
P_{wn}	Nominal wind power [kW]
P_{pvsat}	Nominal photovoltaic power [kW]
P_{cutoff}	Cut off wind power [kW]
P_{g}^{max}	Maximum power balance [kW]
P_{g}^{min}	Minimum power balance [kW]
q_{h}	Penalty for the load curtailment
q_{bat}	Penalty for the battery bank cost
q_{crt}	Penalty for the Critical SOC
q_{dump}	Penalty for the energy waste in the load dump
T_{c}	Time related to the maximum number of grid connections
T_{s}	Sample time [s]
T_{up}	Minimum number of samples for the MG to remain grid connected
T_{down}	Minimum number of samples for the MG to remain isolated
S_{crt}	Critical state of charge [pu]
$S_{\max}$	Maximum state of charge [pu]

S_{max}	Minimum state of charge [pu]
V_b	Battery bank voltage [Volts]
V_{oc}	Open circuit photovoltaic voltage [Volts]
v_n	Nominal wind speed [m/s]
v_{cutin}	Cut-in wind speed [m/s]
v_{cutoff}	Cut-off wind speed [m/s]
x_b^s	Storage auto discharge [pu]
	Real Variables
$c_p(k)$	Energy purchase price [US$/kWh]
$c_s(k)$	Energy sell price [US$/kWh]
$C_g(k)$	Energy purchase or sell cost [US$]
C_{bat}	Total O&M battery bank cost during the scheduling horizon [US$]
$D_{c2}(k)$	Battery charger demand [kW]
$D_{ch}(k)$	Battery charger auxiliary variable [kW]
$D_h(k)$	Demand of controllable loads [kW]
$D_i(k)$	Demand of critical loads[kW]
$D_c(k)$	Total controllable load demand [kW]
$D_c^f(k)$	Total scheduled load demand [kW]
$D_L(k)$	Total load demand [kW]
$I(k)$	Photovoltaic panel current [A]
$i_L(k)$	Total load current [A]
$i_{pv}(k)$	Photovoltaic generator current [A]
$i_w(k)$	Wind turbine generator current [A]
$i_{ch}(k)$	ESS charger current [A]
$J_N(k)$	Objective function
$J_{dis}(k)$	Discomfort costs
J_{dump}	Total waste cost in the dump load during the scheduling horizon [US$]
$J_{bat}(k)$	O&M battery bank costs [US$]
$J_p(k)$	Electricity costs [US$]
J_{pur}	Total cost of purchase electricity the scheduling horizon [US$]
$J_s(k)$	Total revenue from electricity sale during the scheduling horizon [US$]
$\lambda(k)$	Irradiance [W/m^2]
$\xi_s(k)$	Elapse time for the MG stay connected to the main grid [min]
$P_g(k)$	Power balance [kW]
$P_{pv}(k)$	Photovoltaic power [kW]
$P_{pv}^f(k)$	Forecast of the photovoltaic power [kW]
$P_w(k)$	Wind power [kW]
$P_w^f(k)$	Forecast of the wind power [kW]
$profit$	Electricity profit [US$]
PT_{crt}	The percentage rate between T_{crt} and the total simulation time [%]
$S(k)$	State of the battery charge [pu]
$T(k)$	Temperature [^{o}C]
T_{crt}	Total time period that the SOC remains below the critical SOC [min]
$V(k)$	Photovoltaic panel voltage [V]
$v_w(k)$	Wind speed [m/s]
$x_w(k)$	State variable related to the wind power [kW]
$x_{pv}(k)$	State variable related to the photovoltaic power [kW]
	Integer and Binary Variables
$\xi_c(k)$	Integer variable related to the MG-connections counter
$\xi_{hon}(k)$	Integer variable related to the total samples left to enable the MG connection
$\xi_{hoff}(k)$	Integer variable related to the total samples left to enable the MG disconnection
$T_{up}(k)$	Integer variable related to the minimum number of samples required for the MG remains grid connected
$T_{up}(k)$	Integer variable related to the minimum number of samples required for the MG remains isolated
$m_c(k)$	Integer variable related to the mode selector of the timer $\xi_s(k)$
$m_{clk}(k)$	Integer variable related to the mode selector of $\xi_{hon}(k)$ and $\xi_{off}(k)$
$m_{count}(k)$	Integer variable related to the mode selector of the counter $\xi_c(k)$
$m_l(k)$	Integer variable related to the load mode selector
$m_p(k)$	Integer variable related to the mode selector of the energy price
$m_{pv}(k)$	Integer variable related to the mode selector of the photovoltaic generation
$m_w(k)$	Integer variable related to the mode selector of the wind generation
$m_s(k)$	Integer variable related to the mode selector of the battery charge
$c_h(k)$	Binary variable that is enabled when the load h is turned on
$holdoff(k)$	Binary variable that is enabled when MG is in isolated mode
$holdon(k)$	Binary variable that is enabled when MG is grid connected
$\delta_c(k)$	Binary variable that is enabled when there is an MG grid disconnection.
$\delta_{cmax}(k)$	Binary variable that is enabled when the number of grid connections is maximum
$\delta_{\xi}(k)$	Binary variable that is enabled when $\xi_s(k)$ is reseted
$\delta_g(k)$	Binary variable that is enabled when the power balance is positive
$\delta_{dex}(k)$	Complement of $\delta_g(k)$
$\delta_{hon}(k)$	Binary variable that is enabled when the counter $\xi_{hon}(k)$ is negative
$\delta_{hoff}(k)$	Binary variable that is enabled when the counter $\xi_{off}(k)$ is positive
$\delta_{pv1}(k)$	Binary variable that is enabled when the photovoltaic power is saturated
$\delta_{s1}(k)$	Binary variable that is enabled when the battery bank is charged
$\delta_{s2}(k)$	Binary variable that is enabled when the battery bank is not charged and the MG is connected to the grid
$\delta_{wi}(k)$	Binary variables that enables the wind turbine state i
$op(k)$	Binary variable that is enabled when the wind turbine is operating below its rated power
$pn(k)$	Binary variable that is enabled when the wind turbine is operating at its rated power
$u_g(k)$	Binary variable that is enabled when the MG connects to the grid
	Linguistic Variables of the Wind Turbine
$x_{wb}(k)$	Idle,MPPT,Nominal,Cut-off
$x_{wb1}(k)$	Idle state
$x_{wb2}(k)$	MPPT state
$x_{wb3}(k)$	Nominal state
$x_{wb4}(k)$	Cut-off state

Declaration of competing interest

The authors declare that they have no known competing financial interests or personal relationships that could have appeared to influence the work reported in this paper.

Acknowledgments

The authors thank the financial support received from the State of Espirito Santo Research Foundation (FAPES), project number 67666027, and the authorization of the Federal Institute of Education, Science, and Technology of Espirito Santo (IFES) to carry out this research under the process number 23158.001738/2018-33.

Appendix A. Adjustment of the wind speed in the turbine

The height of the wind turbine is different from the height of the weather data station. The real wind speed in the wind turbine is recalculated using a logarithmic profile given by

$$\frac{v}{v_0} = \frac{ln(H/z_0)}{ln(H_0/z_0)} \quad (A.1)$$

where z_0 is the roughness length in meters, H_o is the reference height in meters corresponding to the speed v_o in the weather station, and H is the height in meters corresponding to the speed v in the wind turbine, respectively. For the case study, $H = 15$ m, $H_0 = 10$ m and $z_0 = 1$ m. The height values were obtained at the installation site of the weather stations and wind turbine, and the roughness length was taken from a roughness table [65] classified for urban areas.

Appendix B. Rule-based strategy

The rule-based strategy algorithm consists of the following steps:

1. Monitor the variation rate of the battery charge (SOC) at all n_c operation ranges, where n_c is the number of controllable loads. These ranges define intervals where the SOC variation rates are negative to prevent the battery bank from having a deep discharge.
2. If the SOC's charge rate is in the range $k, k = 1, 2, \ldots, n_c - 1$ and if there are turn on loads, then turn off 1 to k loads gradually, starting from the lower priority and go to step 3. If the SOC variation rate exceeds its lowest value, then turn off all loads and go to step 3. Otherwise, do not turn off the loads and go to step 3.
3. Monitor the SOC state of the batteries and the power balance (difference between the current demand and the generated RES power).
4. Check whether the maximum-allowed number of MG grid connections in a time interval is achieved. In this case, the MG must remain isolated and return to step 1. Otherwise, go to step 5.
5. If the MG is already connected to the grid, then keep it connected for at least T_{up} time periods and then return to step 1. Otherwise, go to the next step.
6. Verify the following connection conditions: (a) The state of the battery bank charge is not at its critical value or (b) The RES power generated is higher than the load demand plus the battery bank charge. If one of the conditions is true, then perform the MG grid connection or keep the MG connected to the grid and return to step 1. Otherwise, perform a grid disconnection or keep it disconnected for a minimum number of samples T_{down} and return to step 1.

References

[1] Production of primary energy. EUROSTAT. URL www.ec.europa.eu/eurostat/statistics-explained/index.php/Energy. [Accessed 18 May 2020].
[2] Electricity in the United States. EIA. URL www.eia.gov/outlooks/aeo/pdf/AEO2020. [Accessed 18 May 2020].
[3] End of the year wrap-up: five figures show China's renewable energy growth in 2019. URL www.renewableenergyworld.com/2019/12/01/end-of-the-year-wrap-up-five-figures-show-chinas-renewable-energy-growth-in-2019. [Accessed 18 May 2020].
[4] Statistical annual of electricity. Energetic Research Company. URL www.epe.gov.br/pt/publicacoes-dados-abertos/publicacoes/anuario-estatistico-de-energia-eletrica. [Accessed 10 May 2020].
[5] Liang H, Zhuang W. Stochastic modeling and optimization in a microgrid: A survey. Energies 2014;7,:2027–50. http://dx.doi.org/10.3390/en7042027.
[6] Nosratabadi SM, Hooshmand RA, Gholipour E. A comprehensive review on microgrid and virtual power plant concepts employed for distributed energy resources scheduling in power systems. Renew Sustain Energy Rev 2017;67,:341–63. http://dx.doi.org/10.1016/j.rser.2016.09.025.
[7] Hossain MA, Pota HR, Hossain MJ, Blaabjerg F. Evolution of microgrids with converter-interfaced generations: Challenges and opportunities. Int J Electr Power Energy Syst 2019;109,:160–86. http://dx.doi.org/10.1016/j.ijepes.2019.01.038.
[8] Gonzalez de Durana J, Barambones O. Technology-free microgrid modeling with application to demand side management. Appl Energy 2018;219,:165–78. http://dx.doi.org/10.1016/j.apenergy.2018.03.024.
[9] Zhang X, Chen B, Cheng Y, Sun S, Wang S. A multi-microgrids system model considering stochastic correlations among microgrids. Energy Procedia 2018;145,:3–8. http://dx.doi.org/10.1016/j.egypro.2018.04.002.
[10] Hanna R, Ghonima M, Kleissl J, Tynan G, Victor DG. Evaluating business models for microgrids: Interactions of technology and policy. Energy Policy 2017;103,:47–61. http://dx.doi.org/10.1016/j.enpol.2017.01.010.
[11] Magro MC, Giannettoni M, Pinceti P, Vanti M. Real time simulator for microgrids. Electr Power Syst Res 2018;160,:381–96. http://dx.doi.org/10.1016/j.epsr.2018.03.018.
[12] Zhu L, Hill DJ. Modeling and stability of microgrids with smart loads. IFAC-PapersOnLine 2017;50,:10021–6. http://dx.doi.org/10.1016/j.ifacol.2017.08.2037.
[13] Parisio A, Rikos E, Glielmo L. A model predictive control approach to microgrid operation optimization. IEEE Trans Control Syst Technol 2014;22,:1813–27. http://dx.doi.org/10.1109/TCST.2013.2295737.
[14] Garcia-Torres F, Bordons C. Optimal economical schedule of hydrogen-based microgrids with hybrid storage using model predictive control. IEEE Trans Ind Electron 2015;62:5195–207. http://dx.doi.org/10.1109/TIE.2015.2412524.
[15] Olama A, Mendes PR, Camacho EF. Lyapunov-Based hybrid model predictive control for energy management of microgrids. IET Gener Transm Distrib 2018;12,:5770–80. http://dx.doi.org/10.1049/iet-gtd.2018.5852.
[16] Bemporad A, Morari M. Control of systems integrating logic, dynamics, and constraints. Automatica 1999;35,:407–27. http://dx.doi.org/10.1016/S0005-1098(98)00178-2.
[17] Elsied M, Oukaour A, Youssef T, Gualous H, Mohammed O. An advanced real time energy management system for microgrids. Energy 2016;114,:742–52. http://dx.doi.org/10.1016/j.energy.2016.08.048.
[18] Kumar RH, Ushakumari S. A novel control strategy for autonomous operation of isolated microgrid with prioritized loads. J Inst Eng India: Ser B 2018;99,:323–30. http://dx.doi.org/10.1007/s40031-018-0335-7.
[19] Wasilewski J. Optimisation of multicarrier microgrid layout using selected metaheuristics. Int J Electr Power Energy Syst 2018;99,:246–60. http://dx.doi.org/10.1016/j.ijepes.2018.01.022.
[20] Gazijahani FS, Salehi J. Integrated DR and reconfiguration scheduling for optimal operation of microgrids using Hong's point estimate method. Int J Electr Power Energy Syst 2018;99,:481–92. http://dx.doi.org/10.1016/j.ijepes.2018.01.044.
[21] Sharma A, Panigrahi BK. Phase fault protection scheme for reliable operation of microgrids. IEEE Trans Ind Appl 2018;54,:2646–55. http://dx.doi.org/10.1109/TIA.2017.2787691.
[22] Herath PU, Fusco V, Caceres MN, Venayagamoorthy GK, Squartini S, Piazza F, et al. Day-ahead power forecasting in a large-scale photovoltaic plant based on weather classification using LSTM. IEEE Trans Ind Appl 2019;55,:732–40. http://dx.doi.org/10.1109/TIA.2018.2871390.
[23] Hossain MA, Pota HR, Squartini S, Abdou AF. Modified PSO algorithm for real-time energy management in grid-connected microgrids. Renew Energy 2019;136,:746–57. http://dx.doi.org/10.1016/j.renene.2019.01.005.
[24] Tenfen D, Finardi EC. A mixed integer linear programming model for the energy management problem of microgrids. Electr Power Syst Res 2015;122,:19–28. http://dx.doi.org/10.1016/j.epsr.2014.12.019.
[25] Liu G, Starke M, Xiao B, Zhang X, Tomsovic K. Microgrid optimal scheduling with chance-constrained islanding capability. Electr Power Syst Res 2017;145,:197–206. http://dx.doi.org/10.1016/j.epsr.2017.01.014.
[26] Li Z, Xu Y. Optimal coordinated energy dispatch of a multi-energy microgrid in grid-connected and islanded modes. Appl Energy 2018;158,:6601–6. http://dx.doi.org/10.1016/j.apenergy.2017.08.197.
[27] Silvente J, Kopanos GM, Pistikopoulos EN, Espuña A. A rolling horizon optimization framework for the simultaneous energy supply and demand planning in microgrids. Appl Energy 2015;155,:485–501. http://dx.doi.org/10.1016/j.apenergy.2015.05.090.
[28] Marquant JF, Evins R, Carmeliet J. Reducing computation time with a rolling horizon approach applied to a MILP formulation of multiple urban energy hub system. Procedia Comput Sci 2015;51,:11. http://dx.doi.org/10.1016/j.procs.2015.05.486.
[29] Javier Silvente VD, Papageorgiou LG. A rolling horizon approach for optimal management of microgrids under stochastic uncertainty. Chem Eng Res 2018;131,:293–317. http://dx.doi.org/10.1016/j.cherd.2017.09.013.

[30] Gu W, Wang Z, Wu Z, Luo Z, Tang Y, Wang J. An online optimal dispatch schedule for CCHP microgrids based on model predictive control. IEEE Trans Smart Grid 2017;8,:2332–42. http://dx.doi.org/10.1109/TSG.2016.2523504.
[31] Alramlawi M, Gabash A, Li P. Optimal operation strategy of a hybrid PV-battery system under grid scheduled blackouts. In: IEEE international conference on environment and electrical engineering and IEEE industrial and commercial power systems europe (EEEIC / I CPS Europe). Milan, Italy; 2017, p. 1–5. http://dx.doi.org/10.1109/EEEIC.2017.7977543.
[32] Romero-Quete D, Garcia JR. An affine arithmetic-model predictive control approach for optimal economic dispatch of combined heat and power microgrids. Appl Energy 2019;242,:1436–47. http://dx.doi.org/10.1016/j.apenergy.2019.03.159.
[33] Resende M, Cardoso V. Mapping service quality in electricity distribution: An exploratory study of Brazil. Util Policy 2019;56,:41–52. http://dx.doi.org/10.1016/j.jup.2018.08.009.
[34] Ismail MS, Moghavvemi M, Mahlia TM, Muttaqi KM, Moghavvemi S. Effective utilization of excess energy in standalone hybrid renewable energy systems for improving comfort ability and reducing cost of energy: A review and analysis. Renew Sustain Energy Rev 2015;42,:726–34. http://dx.doi.org/10.1016/j.rser.2014.10.051.
[35] Khakimova A, Shamshimova A, Sharipova D, Kusatayeva A, Ten V, Bemporad A, et al. Hybrid model predictive control for optimal energy management of a smart house. In: IEEE 15th international conference on environment and electrical engineering. Rome, Italy; 2015, p. 513–8. http://dx.doi.org/10.1109/EEEIC.2017.7977543.
[36] Parisio A, Wiezorek C, Kyntaja T, Elo J, Johansson KH. An MPC-based energy management system for multiple residential microgrids. In: IEEE international conference on automation science and engineering. Gothenburg, Sweden; 2015, p. 7–14. http://dx.doi.org/10.1109/CoASE.2015.7294033.
[37] Bruni G, Cordiner S, Mulone V, Sinisi V, Spagnolo F. Energy management in a domestic microgrid by means of model predictive controllers. Energy 2016;108,:119–31. http://dx.doi.org/10.1016/j.energy.2015.08.004.
[38] Clarke WC, Manzie C, Brear MJ. An economic MPC approach to microgrid control. In: Australian control conference. Newcastle, NSW, Australia; 2017, p. 276–81. http://dx.doi.org/10.1109/AUCC.2016.7868202.
[39] Pereira M, Muñoz de la Peña D, Limon D. Robust economic model predictive control of a community micro-grid. Renew Energy 2017;100,:3–17. http://dx.doi.org/10.1016/j.renene.2016.04.086.
[40] Zheng Y, Li S, Tan R. Distributed model predictive control for on-connected microgrid power management. IEEE Trans Control Syst Technol 2017;26,:1–12. http://dx.doi.org/10.1109/TCST.2017.2692739.
[41] Parisio A, Rikos E, Glielmo L. Stochastic model predictive control for economic/environmental operation management of microgrids: An experimental case study. J Process Control 2016;43,:24–37. http://dx.doi.org/10.1016/j.jprocont.2016.04.008.
[42] Agüera-Pérez A, Palomares-Salas JC, González de la Rosa JJ, Florencias-Oliveros O. Weather forecasts for microgrid energy management: Review, discussion and recommendations. Appl Energy 2018;228,:265–78. http://dx.doi.org/10.1016/j.apenergy.2018.06.087.
[43] Eseye AT, Zhang J, Zheng D. Short-term photovoltaic solar power forecasting using a hybrid wavelet-PSO-SVM model based on SCADA and meteorological information. Renew Energy 2018;118,:357–67. http://dx.doi.org/10.1016/j.renene.2017.11.011.
[44] Skamarock W, Klemp J, Dudhia J, Gil D, Liu Z, Berner J, et al. A description of the advanced research WRF model version 4. National Center for Atmospheric Research; 2019.
[45] D. E. Olivares CAC, Kazerani M. Stochastic-predictive energy management system for isolated microgrids. IEEE Trans Smart Grid 2015;6,:2681–93. http://dx.doi.org/10.1109/TSG.2015.2469631.
[46] Palma-Behnke R, Benavides C, Lanas F, Severino B, Reyes L, Llanos J, et al. A microgrid energy management system based on the rolling horizon strategy. IEEE Trans Smart Grid 2013;4,:996–1006. http://dx.doi.org/10.1109/TSG.2012.2231440.
[47] Silva DP, Queiroz MD, Fardin JF, Sales JLF, Orlando MTD. Hybrid modeling of energy storage system and electrical loads in a pilot-microgrid. In: 13th IEEE International Conference on Industry Applications. São Paulo, Brazil; 2018, p. 433–8. http://dx.doi.org/10.1109/INDUSCON.2018.8627180.
[48] Kang BO, Park JH. Kalman filter MPPT method for a solar inverter. In: IEEE power and energy conference at Illinois. Urbana, IL, USA; 2011, p. 1–5. http://dx.doi.org/10.1109/EEEIC.2017.7977543.
[49] Yan X, Abbes D, Francois B. Uncertainty analysis for day ahead power reserve quantification in an urban microgrid including PV generators. Renew Energy 2017;106,:288–97. http://dx.doi.org/10.1016/j.renene.2017.01.022.
[50] Marinelli M, Sossan F, Costanzo GT, Bindner HW. Testing of a predictive control strategy for balancing renewable sources in a microgrid. IEEE Trans Sustain Energy 2014;5,:1426–33. http://dx.doi.org/10.1109/TSTE.2013.2294194.
[51] Shi YT, Qiao SJ, Hou YJ, Li ZJ, Sun DH. Hybrid model predictive control and fault detection of wind energy conversion system based on mixed logical dynamic. In: 26th chinese control and decision conference. Changsha, China; 2014, p. 782–8. http://dx.doi.org/10.1109/CCDC.2014.6852271.
[52] Bemporad A, Torrisi F, Morari M. Discrete-time hybrid modeling and verification of the batch evaporator process benchmark. Eur J Control 2001;0,:1–18. http://dx.doi.org/10.3166/ejc.7.382-399.
[53] Olivares DE, Mehrizi-Sani A, Etemadi AH, Cañizares CA, Iravani R, Kazerani M, et al. Trends in microgrid control. IEEE Trans Smart Grid 2014;5,:1905–19. http://dx.doi.org/10.1109/TSG.2013.2295514.
[54] El-Hendawi M, Gabbar H, El-Saady G, Ibrahim E-N. Control and EMS of a grid-connected microgrid with economical analysis. Energies 2018;11,:20. http://dx.doi.org/10.3390/en11010129.
[55] Mazidi M, Zakariazadeh A, Jadid S, Siano P. Integrated scheduling of renewable generation and demand response programs in a microgrid. Energy Convers Manage 2014;86,:1118–27. http://dx.doi.org/10.1016/j.enconman.2014.06.078.
[56] Crystalline photovoltaic modules installation and operation manual. 2017, URL www.axitecsolar.com/data/document_files/Manual_PT.pdf. [Accessed 21 May 2020].
[57] Fronius galvo 208-240 operating instructions. 2016, URL www.fronius.com/~/downloads/Solar%20Energy/Operating%20Instructions/42%2C0410%2C1934.pdf. [Accessed 21 May 2020].
[58] GERAR 246 instructions manual. 2016, URL http://www.enersud.com.br/produtos/turbina-eolica-gerar-246/. [Accessed 21 June 2020].
[59] Wind grid tie inverter GCI-2G-W single phase inverter, installation and operation manual. 2018, URL http://ginlong.com/Download/down/id/527.html. [Accessed 06 November 2018].
[60] Stationary battery technical manual clean nano. 2016, URL www.moura-portal.s3.amazonaws.com/uploads/2017/07/MANUAL_CLEAN_NANO_V13_06_DEZ_16.pdf. [Accessed 21 May 2020].
[61] National Institute of Meteorology. INMET. www.inmet.gov.br/portal/index.php?r=estacoes/estacoesAutomaticas. [Accessed 10 May 2020].
[62] Caplan P, Derber J, Gemmill W, Hong SY, Pan HL, Parrish D. Changes to the 1995 NCEP operational medium-range forecast model analysis-forecast system. Weather Forecast 1997;12,:581–94. http://dx.doi.org/10.1175/1520-0434(1997)012<0581:CTTNOM>2.0.CO;2.
[63] IEEE application guide for IEEE Std 1547(TM), IEEE standard for interconnecting distributed resources with electric power systems, IEEE Std 1547-2018. 2018, p. 1–217.
[64] de Oliveira Junior VB, Pena JG, Salles JL. An improved plant-wide multiperiod optimization model of a byproduct gas supply system in the iron and steel-making process. Appl Energy 2016;164,:462–74. http://dx.doi.org/10.1016/j.apenergy.2015.11.043.
[65] Masters GM. Renewable and efficient electric power systems. 2nd ed. John Wiley and Sons; 2013.